Bottomless Culvert Scour Study: Phase II Laboratory Report

PUBLICATION NO. FHWA-HRT-07-026

FEBRUARY 2007

U.S. Department of Transportation
Federal Highway Administration

Research, Development, and Technology
Turner-Fairbank Highway Research Center
6300 Georgetown Pike
McLean, VA 22101-2296

Foreword

The bottomless culvert study described in this report was conducted at the Federal Highway Administration (FHWA) hydraulics laboratory in response to a request by the Maryland State Highway Administration (MDSHA) in a partnership arrangement in which MDSHA shared the cost of the study. A primary objective of this study was to validate or improve an existing methodology developed by MDSHA for estimating scour in bottomless culverts. The study included experiments to determine stability of rock riprap and to test effectiveness of rock cross vanes and other measures to reduce scour at the foundations of bottomless culverts. This report will be of interest to hydraulic engineers and bridge engineers who are involved in selection and design of structures for small stream crossings. It is being distributed as an electronic document through the Turner-Fairbank Highway Research Center Web site (www.tfhrc.gov).

Gary L. Henderson, P.E.
Director, Office of Infrastructure
Research and Development

Notice

Quality Assurance Statement

The Federal Highway Administration (FHWA) provides high-quality information to serve Government, industry, and the public in a manner that promotes public understanding. Standards and policies are used to ensure and maximize the quality, objectivity, utility, and integrity of its information. FHWA periodically reviews quality issues and adjusts its programs and processes to ensure continuous quality improvement.

Technical Report Documentation Page

1. Report No. FHWA-HRT-07-026	2. Government Accession No.	3. Recipient's Catalog No.
4. Title and Subtitle Bottomless Culvert Scour Study: Phase II Laboratory Report		5. Report Date February 2007 6. Performing Organization Code
7. Author(s) Kornel Kerenyi, J. Sterling Jones, and Stuart Stein		8. Performing Organization Report No.
9. Performing Organization Name and Address GKY and Associates, Inc. 5411-E Backlick Road Springfield, VA 22151		10. Work Unit No. (TRAIS) 11. Contract or Grant No.
12. Sponsoring Agency Name and Address Office of Infrastructure Research and Development Federal Highway Administration 6300 Georgetown Pike McLean, VA 22101-2296		13. Type of Report and Period Covered Laboratory Report May 2002–November 2005 14. Sponsoring Agency Code

15. Supplementary Notes

Contracting Officer's Technical Representative (COTR): J. Sterling Jones, HRDI-07

The Maryland State Highway Administration (MDSHA) provided technical assistance and partial funding for this study. Dr. Fred Chang was instrumental in setting up the experimental plan and provided a data analysis strategy. Dr. Larry Arneson and Jorge E. Pagán-Ortiz provided technical review of this document.

16. Abstract

Bottomless culverts are three-sided structures that use the natural channel for the bottom. These structures could be used to convey flows from one side of a highway to the other. As such, they are an environmentally attractive alternative to box, pipe, and pipe arch culvert designs. Bottomless culverts range in size from less than a meter (1.5 feet) to more than 10 meters (35 feet) in width. The failure of such a structure could have severe consequences similar to the failure of a bridge. On the other hand, since the cost of the foundation and scour countermeasures represents a significant portion of the cost of this type of structure, overdesign of these elements can add significantly to the cost of the project.

Several dozen physical modeling configurations of bottomless culverts were tested, and the resulting scour at the entrance along the foundation and outlet was measured. Predictive equations for estimating scour depth were developed and compared to MDSHA methodology. These equations will provide guidance for the design of footing depths for bottomless culverts.

The study was conducted in two phases. The first phase focused on measuring maximum scour depths at the culvert entrance and developing an analysis procedure using methods found in the literature to approximate prescour hydraulic parameters that drive the analysis. No fixed-bed experiments were conducted in the first phase to measure actual prescour hydraulic parameters. No submerged entrance experiments were conducted in the first phase. The second phase expanded the investigation to include scour measurements at the outlet, submerged entrance scour measurements, and detailed velocity and depth measurements with a prescour fixed bed at locations where maximum scour occurred. Additional tests were conducted to evaluate the use of various measures to reduce scour including wingwalls, pile dissipators, riprap, and cross vanes.

Phase I results are reported in Kerenyi, K., Jones, J.S., and Stein, S., *Bottomless Culvert Scour Study: Phase I Laboratory Report*, FHWA-RD-02-078, 2003.

17. Key Words	18. Distribution Statement
Scour, culverts, hydraulics, physical model.	No restrictions. This document is available to the public through the National Technical Information Service (NTIS), Springfield, VA 22161.

19. Security Classif. (of this report)	20. Security Classif. (of this page)	21. No. of Pages	22. Price
Unclassified	Unclassified	77	

SI* (MODERN METRIC) CONVERSION FACTORS

APPROXIMATE CONVERSIONS TO SI UNITS

Symbol	When You Know	Multiply By	To Find	Symbol
		LENGTH		
in	inches	25.4	millimeters	mm
ft	feet	0.305	meters	m
yd	yards	0.914	meters	m
mi	miles	1.61	kilometers	km
		AREA		
in^2	square inches	645.2	square millimeters	mm^2
ft^2	square feet	0.093	square meters	m^2
yd^2	square yard	0.836	square meters	m^2
ac	acres	0.405	hectares	ha
mi^2	square miles	2.59	square kilometers	km^2
		VOLUME		
fl oz	fluid ounces	29.57	milliliters	mL
gal	gallons	3.785	liters	L
ft^3	cubic feet	0.028	cubic meters	m^3
yd^3	cubic yards	0.765	cubic meters	m^3
		NOTE: volumes greater than 1000 L shall be shown in m^3		
		MASS		
oz	ounces	28.35	grams	g
lb	pounds	0.454	kilograms	kg
T	short tons (2000 lb)	0.907	megagrams (or "metric ton")	Mg (or "t")
		TEMPERATURE (exact degrees)		
^oF	Fahrenheit	5 (F-32)/9 or (F-32)/1.8	Celsius	^oC
		ILLUMINATION		
fc	foot-candles	10.76	lux	lx
fl	foot-Lamberts	3.426	$candela/m^2$	cd/m^2
		FORCE and PRESSURE or STRESS		
lbf	poundforce	4.45	newtons	N
lbf/in^2	poundforce per square inch	6.89	kilopascals	kPa

APPROXIMATE CONVERSIONS FROM SI UNITS

Symbol	When You Know	Multiply By	To Find	Symbol
		LENGTH		
mm	millimeters	0.039	inches	in
m	meters	3.28	feet	ft
m	meters	1.09	yards	yd
km	kilometers	0.621	miles	mi
		AREA		
mm^2	square millimeters	0.0016	square inches	in^2
m^2	square meters	10.764	square feet	ft^2
m^2	square meters	1.195	square yards	yd^2
ha	hectares	2.47	acres	ac
km^2	square kilometers	0.386	square miles	mi^2
		VOLUME		
mL	milliliters	0.034	fluid ounces	fl oz
L	liters	0.264	gallons	gal
m^3	cubic meters	35.314	cubic feet	ft^3
m^3	cubic meters	1.307	cubic yards	yd^3
		MASS		
g	grams	0.035	ounces	oz
kg	kilograms	2.202	pounds	lb
Mg (or "t")	megagrams (or "metric ton")	1.103	short tons (2000 lb)	T
		TEMPERATURE (exact degrees)		
^oC	Celsius	1.8C+32	Fahrenheit	^oF
		ILLUMINATION		
lx	lux	0.0929	foot-candles	fc
cd/m^2	$candela/m^2$	0.2919	foot-Lamberts	fl
		FORCE and PRESSURE or STRESS		
N	newtons	0.225	poundforce	lbf
kPa	kilopascals	0.145	poundforce per square inch	lbf/in^2

*SI is the symbol for the International System of Units. Appropriate rounding should be made to comply with Section 4 of ASTM E380.
(Revised March 2003)

TABLE OF CONTENTS

LIST OF FIGURES

LIST OF TABLES

LIST OF SYMBOLS

A_k	dimensionless ratio: area of approaching flow directly above culvert divided by total area of flow approaching culvert.
A_{CULV}	cross sectional area of flow in the culvert.
C	calibration coefficient for determining V_{RM}.
D	height of culvert at approach prior to scour.
D_{50}	sediment size.
E	Ishbash constant.
F_1	Froude number at culvert approach.
F_o	Froude number in contraction zone.
g	acceleration of gravity.
kp	empirical coefficient needed to explain additional scour depth caused by pressure flow at a submerged culvert.
ks	empirical coefficient needed to explain additional scour depth caused by spiral flow at culvert toe.
k_v	ratio of velocity at the culvert toe to the mean velocity in the contracted section.
k_{vadj}	kv with a calibration coefficient, C.
K_{RIP}	coefficient used to size riprap for scour.
Ku	6.19 for SI units, or 11.17 for U.S. customary units.
K_U	0.55217 for SI units, or 1.0 for U.S. customary units.
K_{U1}	$0.3048^{(0.65-x)}$ for SI units, or 1.0 for U.S. customary units.
K_{U2}	0.788 for SI units, or 1.0 for U.S. customary units.
KVM	coefficient relating local bed velocity in experiments to average velocity in contraction zone.
N_{SC}	computed sediment number for distributed flow.
q_1	unit discharge in the approach section.
q_2	unit discharge in the contracted section.
q_R	assumed representative unit discharge across the scour hole at the beginning of scour.
Q	volumetric flow rate.
$Q_{blocked}$	portion of approach flow that is to one side of channel centerline and blocked by the embankment as flow approaches culvert.
SG	specific gravity of riprap.
$R_{Qblocked}$	dimensionless ratio that includes $Q_{blocked}$ and y_2.
V_{AC}	average velocity in the contracted zone prior to scour in the vicinity of the upstream corner of a culvert.
V_C	critical velocity at which incipient sediment motion occurs.
V_{CL}	Laursen's critical velocity.
V_{CN}	Neill's critical velocity.
V_{eff}	effective velocity that accounts for turbulence and vorticity in the mixing zone at the upstream corner of a culvert.
V_{LB}	local velocity along the bed prior to scour in the vicinity of the upstream corner of a culvert.
V_{max}	maximum velocity that rolls out the stones lying among others on a slope.

V_{min}	minimum velocity that removes the loose stones lying on top of fill.
V_R	representative (local) velocity at culvert entrance.
V_{RA}	average velocity.
V_{RP}	representative velocity from potential flow principles..
V_{RM}	measured velocity.
w_a	width of approach channel.
w_{CULV}	width of culvert.
y_0	water depth at the culvert entrance before scour occurs.
y_1	water depth in the approach channel at a distance three times w_{CULV} upstream of the culvert entrance.
y_2	equilibrium water depth after scour hole develops.
y_{max}	maximum water depth in the culvert after scour hole develops.
y_s	maximum depth of scour in the culvert.

ABBREVIATED GLOSSARY

ASCE	American Society of Civil Engineers
EGL	energy grade line
HGL	hydraulic grade line
MDSHA	Maryland State Highway Administration
PIV	particle image velocimetry
SI	International System of Units
VI	virtual instruments
ww	wingwall

1. INTRODUCTION

Bottomless (or three-sided) culverts use the natural channel bed and are environmentally attractive alternatives to traditional closed culverts. Moreover, they are often promoted as alternatives for replacing short bridges. These structures are typically founded (supported) on spread footings, and the issue of scour and the depth of footing must be addressed as part of their design. Many State highway agencies will not allow bottomless culverts unless they can be founded on solid rock formations. Therefore, there is a need to formulate a defendable procedure for estimating scour depths in other types of soil formations (e.g., sands). The scour problem is analogous to abutment and contraction scour in a bridge opening and can be treated in much the same manner.

This report describes a two-phase study conducted at the Federal Highway Administration's (FHWA) J. Sterling Jones Hydraulic Laboratory at the request of the Maryland State Highway Administration (MDSHA) in a partnership arrangement. Phase I was a preliminary investigation focused on measuring maximum scour depths at the culvert entrance and developing equations for estimating inlet scour.[1] Phase II was a follow-up investigation to include scour measurements at the outlet, submerged entrance scour measurements, detailed velocity and depth measurements with a prescour fixed bed to refine the equations, and evaluation of various potential scour countermeasures to reduce scour at the culvert inlet and outlet.

One of the objectives of the Phase II study was to compare the MDSHA methodology for determining scour at bottomless culverts with physical modeling data from various culvert configurations. Data from both phases were included in the comparison. In Phase I, models of the typical configurations used for highway applications provided by two commercial suppliers of bottomless culverts were compared to simple rectangular models to gain insight about the effect of culvert shape.[1] In Phase II, simple rectangular shapes were used for the experiments.

Since abutment scour estimates at bridge openings are often quite large, a scour protection task was included to investigate possible scour countermeasures. Various inlet and outlet wingwall configurations were tested. Equations to determine the sizes of rock riprap (rough stones placed to prevent scour) that might be required to reduce scour in the most critical zones were developed. Cross vanes (upstream angled lines of boulders, connected by sections of smaller rocks) and pile flow dissipators (arrays of circular piles buried below the channel bed) were also investigated as scour countermeasures.

While presenting status reports to drainage engineers at American Association of State Highway and Transportation Officials (AASHTO) meetings and at hydraulic conferences, FHWA officials found widespread interest in this topic. The intent of this report is to share the results of this study with a larger audience.

2. EXPERIMENTAL APPROACH

TEST FACILITIES AND INSTRUMENTATION

The experiments were conducted in the FHWA's J. Sterling Jones Hydraulics Laboratory, located at the Turner-Fairbank Highway Research Center in McLean, VA. Test facilities and instrumentation used for the experiments are described in this section.

Figure 1. Photo. View of the flume in the Hydraulics Laboratory.

Hydraulic Flume

The experiments were conducted in a 21.34- by 1.83-meter (m) (70- by 6-feet (ft)) rectangular flume with a 2.4- by 1.83-m (8- by 6-ft) recessed section to allow for scour hole formation (figure 1). A 9.14-m (30-ft) approach section from the head box to the test section consisted of a plywood floor constructed 0.1 m (4 inches) above the stainless steel flume bottom. The plywood floor was coated with a layer of epoxy paint and sand to approximate the roughness of the sand bed in the test section. The walls of the flume were made of a smooth glass. The flume was set at a constant slope of 0.04 percent, and the depth of flow was controlled with an adjustable tailgate located at the downstream end of the flume. Flow was supplied by a 0.3-cubic meter per second (m^3/s) (10-cubic

foot per second (ft^3/s)) pumping system. The discharge was measured with an electromagnetic flow meter.

Electromagnetic Velocity Meter Operation

A 13-millimeter (mm) (0.507-inch) spherical electromagnetic velocity sensor (Marsh-McBirney 523) was used to measure equivalent two-directional mean velocities in a plane parallel to the flume bed. A fluctuating magnetic field was produced in the fluid surrounding the spherical sensor that was orthogonal to the plane of four carbon-tipped electrodes. As a conductive fluid passed around the sensor, an electric potential was produced proportional to the product of the fluid velocity component tangent to the surface of the sphere and normal to the magnetic field and the magnetic field strength. The four carbon-tipped electrodes detected the voltage potential created by the flowing water. The voltage potential produced was proportional to the velocity of the fluid flowing in the plane of the electrodes. Two orthogonal velocity components in the plane of the electrodes were measured.

Particle Image Velocimetry

Particle image velocimetry (PIV) was used to verify and modify the prescour velocity field assumptions and equations developed by Chang (i.e., V_R-values as presented in Phase I of the study).[1] These experimental results were then used to derive new regression equations for the maximum depth of scour and for riprap design.

Postprocessing and Data Analysis

Postprocessing and data analysis were performed using the LabVIEW™ graphical programming technique for building applications such as testing and measurement, data acquisition, instrument control, data logging, measurement analysis, and report generation. LabVIEW programs are called virtual instruments (VIs) because their appearance and operation imitate physical instruments such as oscilloscopes and multimeters. Every VI uses functions that manipulate input from the user interface or other sources and displays that information or moves it to other files or other computers.

MODEL BOTTOMLESS CULVERT SHAPES

Phase I

Three bottomless culvert shapes were constructed and tested: (1) a rectangular model with a width of 0.61 m (2 ft) and a height of 0.46 m (1.5 ft), (2) a CON/SPAN® model with a width of 0.61 m and a height of 0.45 m (1.46 ft), and (3) a CONTECH® model with a width of 0.61 m and a height of 0.42 m (1.36 ft).[1] All three models were evaluated with 45-degree wingwalls and without wingwalls. The models were constructed of Plexiglas®. Marine plywood was used for the headwalls and wingwalls of the models. The models were mounted in the centerline of the flume. The data derived

from testing these culvert shapes were part of the dataset that was used to test the MDSHA (Chang) Method.

Phase II

The laboratory model for this phase consisted of a rectangular bottomless culvert with a width of 0.60 m (2 ft) and a height of 0.15 m (0.49 ft) that was mounted in the centerline of the flume. Figure 2 shows that the culvert and headwall of the model was constructed of Plexiglas or marine plywood, and that the wingwalls were made from marine plywood, Plexiglas, or foam. This model was used to evaluate the outlet scour for a variety of wingwall angles.

Figure 2. Photo. Rectangular culvert.

EXPERIMENTAL PARAMETERS

Approach Flow and Sediment Sizes

Steady flow experiments were conducted for approach flow depths ranging from 0.102 m to 0.325 m (0.33 ft to 1.1 ft) and approach velocities ranging from 0.041 to 0.366 m/s (0.13 to 1.2 ft/s). The discharges to obtain the approach flow conditions varied from approximately 0.024 to 0.14 m^3/s (0.9 to 5 ft^3/s). The particle size (D_{50}) used during the Phase I scour experiments varied from 1.2 to 3.0 mm (0.047 to 0.117 inches). The particle size for Phase II was 1.2 mm (0.047 inches).

Outlet Scour

Steady flow experiments were conducted for approach flow depths ranging from 0.10 to 0.23 m (0.33 to 0.75 ft) and approach velocities ranging from 0.07 to 0.16 m/s (0.23 to

0.52 ft/s). The discharges to obtain the approach flow conditions varied from approximately 0.026 to 0.080 m^3/s (0.9 to 3 ft^3/s). The particle size (D_{50}) was set at 2.0 mm (0.078 inches) for the outlet scour experiments. Several scour countermeasure configurations were tested, including varying wingwall angles, the use of pile dissipators, and the MDSHA Standard Plan, which employs wingwalls at the inlet and outlet of the culvert and lines the wingwalls and the inside walls of the culvert with riprap having a particle size (D_{50}) of 25.4 mm (1 inch).

Riprap Experiments

Riprap experiments were conducted for uniform particle sizes of 12 and 16 mm (0.47 and 0.62 inch). The velocity was increased incrementally until discernible areas of particles were dislodged, which was considered to define the failure condition for that particle size. Because of time constraints, riprap experiments (figure 3) were conducted for the rectangular culvert with vertical headwalls only. Vertical headwalls were considered a worst-case condition, and wingwalls should reduce the riprap size determined from these experiments.

Figure 3. Photo. Riprap test for a rectangular culvert.

Cross Vane Analysis

For the analysis of the cross vanes, the flow velocity was set at 0.17 m/s (0.557 ft/s) and the flow depth was set at 0.152 m (0.5 ft). The particle size (D_{50}) was set at either 0.3 mm (0.012 inch) or 25.4 mm (1 inch). The model scale was 1:12.

Test Matrix

The scour, riprap, and cross vane experiments for bottomless culverts are summarized in the test matrix in table 1.

Table 1. Test matrix for bottomless culvert experiments.

Phase	Experiment	No. of Variations	Comments
I	Various culvert shapes	3	Used two commercially available shapes plus a simple rectangular model
I	Sediment sizes	3	D_{50} varied from 1.2 to 3.0 mm (0.042 to 0.118 inch)
I	Rock riprap stability	—	Used randomly selected gravel retained on a standard sieve to model riprap at the culvert entrance
II	Outlet Scour (Movable Bed) Submerged Inlet	21	Varied wingwall configurations, used pile dissipator, used MDSHA Standard Plan
II	Outlet Scour (Movable Bed) Unsubmerged Inlet	18	Varied wingwall configurations
II	Fixed-Bed Submerged Inlet	19	Investigated local velocities at entrance, with and without wingwalls
II	Fixed-Bed Unsubmerged Inlet	24	Investigated local velocities at entrance, With and without wingwalls
II	PIV	6	Detailed flow investigation at the entrance, small-scale experiments
II	Riprap	4	Varied 3 different sizes of riprap
II	Cross Vanes	5	Varied distance from inlet

3. THEORETICAL BACKGROUND

Experiments show that scour is generally deepest near the corners at the upstream entrance to the culvert. This observation is commonly attributed to the contraction (concentration) of flow near the upstream entrance of the culvert. Figure 4 illustrates the pattern of primary flow near this location, where water that is blocked by the embankments (in the approach to the culvert) is forced through the culvert opening. The vortices and strong turbulence just downstream of the culvert inlet, generated by the contraction of flow and typically called secondary flow, occur in the so-called separation zone. This flow pattern is very similar to the abutment scour phenomenon that researchers have observed for bridge scour.

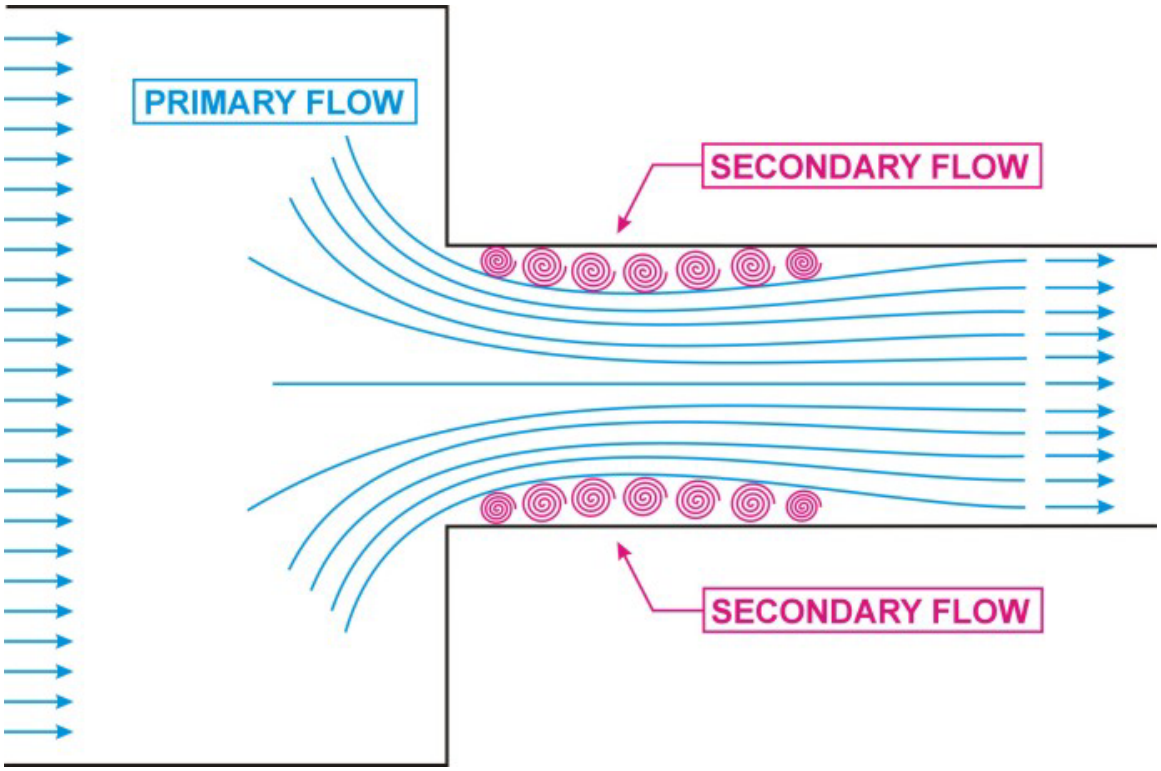

Figure 4. Diagram. Flow concentration and separation zone.

Several researchers, including Chang, GKY and Associates, Inc., and Sturm, have suggested that bridge abutment scour can be analyzed as a form of flow distribution scour by incorporating an empirical adjustment factor to account for vorticity and turbulence.[2,3,4] The adjustment factor to account for vorticity and turbulence can be derived from laboratory results. These notions were used to formulate the theoretical background for analyzing the culvert scour data. Variables used in the data analysis are illustrated in the following definition sketches for unsubmerged (figures 5and 6) and submerged (pressure) (figures 7 and 8) flow conditions. The notations in these figures are defined after the last figure.

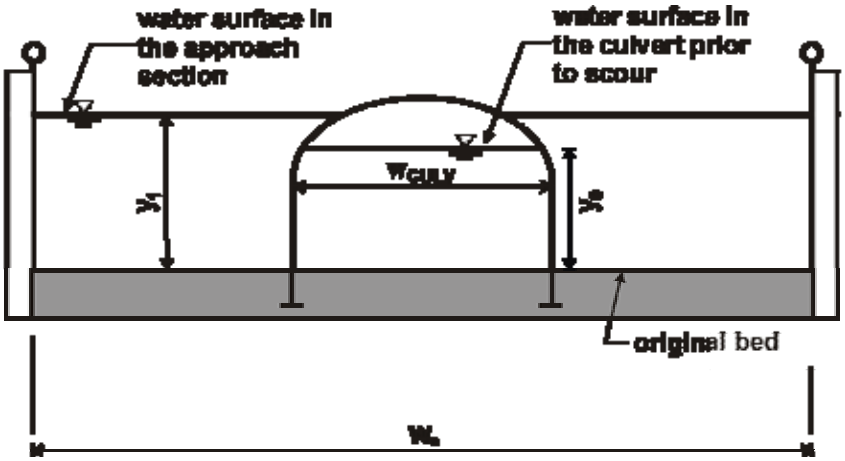

Figure 5. Diagram. Definition sketch before scour for unsubmerged flow conditions.

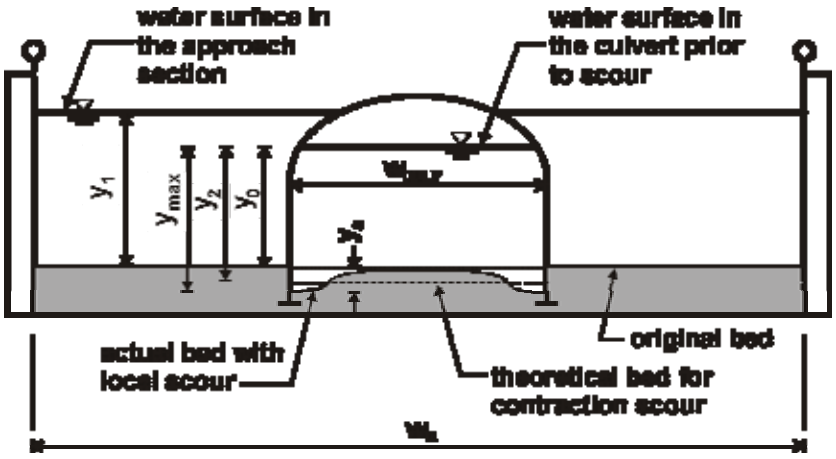

Figure 6. Diagram. Definition sketch after scour for unsubmerged flow conditions.

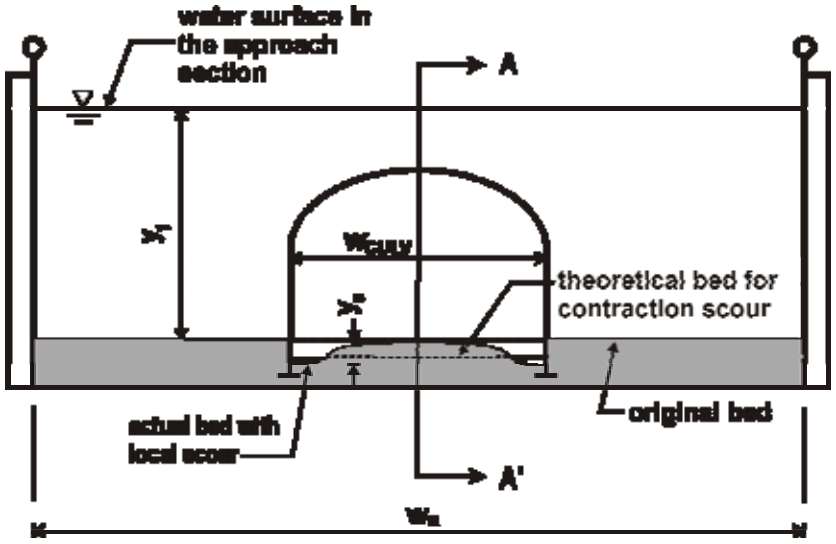

Figure 7. Definition sketch after scour for submerged flow conditions

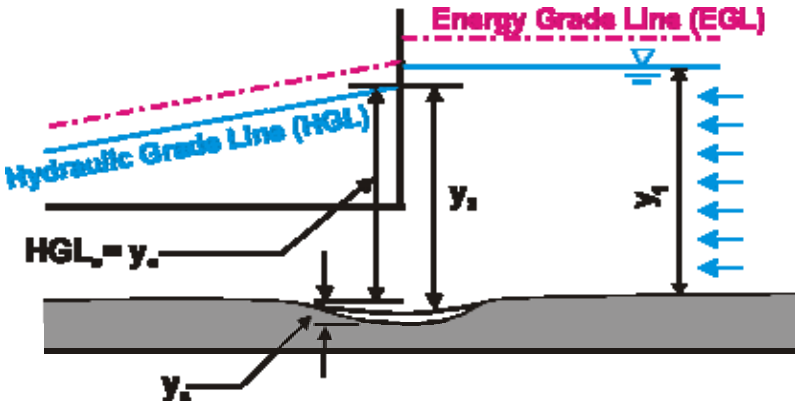

Figure 8. Diagram. Side view after scour for submerged flow conditions (Section A-A′ in figure 7).

w_{CULV}	is width of the culvert.
w_a	is width of the approach channel.
y_1	is water depth in the approach channel at a distance three times w_{CULV} upstream of the culvert entrance.
y_0	is water depth at the culvert entrance before scour occurs.
y_{max}	is maximum water depth in the culvert after scour hole develops.
y_2	is equilibrium water depth after scour hole develops.
y_S	is maximum depth of scour in the culvert.

CLEAR WATER SCOUR

Equation 1 is an expression for the unit discharge for an assumed flow distribution that remains constant as the scour hole develops. If no sediment is being transported into the scour hole, as was the case with all of our experiments, then no sediment can be transported out of the scour hole at equilibrium. In this case, the local velocity must be reduced to the critical incipient motion velocity, V_c, for the sediment size at the equilibrium flow depth, y_2. This equation forms the basis for the analysis:

$$V_R y_0 = V_C y_2 \quad (1)$$

where:

V_R	is representative (local) velocity at the entrance of the culvert.
V_C	is critical velocity at which incipient sediment motion occurs.

Note that the term on the left side of the equation is the assumed representative unit discharge across the scour hole at the beginning of scour, or q_R.

Equation 1 can be rearranged to yield an equilibrium flow depth, y_2, once the representative velocity, V_R, and the critical incipient motion velocity, V_C, have been determined. This equilibrium depth reflects the scour that is attributed to the incoming flow distribution. The next two subsections will illustrate several ways to calculate the

representative velocity and critical velocity. The third and fourth subsections will then discuss two different adjustments to the equilibrium clear water scour depth.

Representative Velocity

Three alternative equations for the representative velocity were considered in this research: the average velocity in the culvert inlet, the potential flow velocity, and finally the measured flow velocity.

Average Flow Velocity

The ABSCOUR program of the MDSHA uses the average velocity in the culvert for the representative velocity.[5] This average velocity, V_{RA}, is just the volumetric flow rate (Q) divided by the cross sectional area of flow in the culvert (A_{CULV}), as in equation 2.

$$V_{RA} = \frac{Q}{A_{CULV}} = \frac{Q}{y_0 w_{CULV}} \tag{2}$$

Potential Flow Theory

Chang used potential flow principles to derive a velocity adjustment expression to approximate the representative velocity (V_{RP}) that should be used for bridge abutment scour computations.[2] This adjustment compensates for the contraction in flow at the culvert inlet. His expression can be adapted for bottomless culverts, as in equation 3.

$$V_{RP} = k_V V_{RA} = \left[0.8 \left(\frac{q_1}{q_2} \right)^{1.5} + 1 \right] \left[\frac{Q}{y_0 w_{CULV}} \right] \tag{3}$$

where:

k_V is the ratio of velocity at the culvert toe to the mean velocity in the contracted section.
q_1 is unit discharge in the approach section.
q_2 is unit discharge in the contracted section.

Equation 3 applies to a simple contraction, where the unit discharge of the approach section, q_1, is less than the unit discharge in the contraction section, q_2. The ABSCOUR program states that the values of k_v should be limited to the range of values between 1.0 and 1.8.[5] If the computed value is less than 1.0, use a value of 1.0; if the computed value is greater than 1.8, use a value of 1.8.

Measured Flow Velocity

Since this research produced accurate measurements of the local velocities in the approach section of the culvert, an adjustment was made to the potential flow theory to

match the measured flow velocity at the corners of the culvert inlet. This adjustment involved adding a calibration coefficient, *C*, as given in equation 4.

$$V_{RM} = k_{Vadj} V_{RA} = C\left[0.8\left(\frac{q_1}{q_2}\right)^{1.5} + 1\right]\left[\frac{Q}{y_0 w_{CULV}}\right] \quad (4)$$

Critical Velocity

There are two alternatives for calculating the critical velocity at which incipient sediment motion occurs that are considered in this report: Laursen's method, and Neill's method.

Laursen's Critical Velocity Method

Laursen's equation for the critical velocity is summarized in Appendix C of FHWA Hydraulic Engineering Circular No. 18.(6) The critical velocity, V_{CL}, is calculated by equation 5.

$$V_{CL} = K_u \, y_2^{1/6} D_{50}^{1/3} \quad (5)$$

where:

K_u is 6.19 for SI units, or 11.17 for U.S. customary units.
y_2 is equilibrium scour flow depth (m or ft).
D_{50} is sediment size (m or ft).

Neill's Competent Velocity Method

Neill presented a family of curves for estimating critical velocities for noncohesive sediments for varying flow depths and with grain sizes ranging from 0.3 to 300 mm (0.0117 to 11.7 inches).(7) Neill defined the critical velocity as the flow velocity just competent to move the bed material. Neill used a combination of field data and laboratory data to develop his family of curves. To develop the family of curves, Neill used a critical velocity equation very similar to Laursen's to estimate the critical velocity for grain sizes greater than about 30 mm (1.17 inches). For a grain size of 0.3 mm (0.0117 inch), Neill assumed that a regime theory equation for stable channels in sand would be appropriate for estimating the critical velocity. (Regime theory equations are design equations developed from field data collected in the stable, fine sediment canals of Pakistan (Mahmood and Shen)).(8) Having defined critical velocities for a grain size of 0.3 mm (0.0117 inch) and for grain sizes greater than 30 mm (1.17 inches), transition curves were hand drawn for grain sizes between 0.3 and 30 mm (0.0117 and 1.17 inches).

Chang transformed the plots of Neill's curves into a set of equations for computing critical velocity based on the flow depth and the median diameter of the particle.(2) This set is given in equations 6 through 9.

For D_{50} greater than 0.03 m (0.1 ft), Neill's critical velocity, V_{CN}, is given in equation 6.

$$V_{CN} = K_U 11.5\, y_2^{1/6} D_{50}^{1/3} \tag{6}$$

where:

y_2 is equilibrium scour flow depth (m or ft).
D_{50} is sediment size (m or ft).
K_U is 0.55217 for SI units, or 1.0 for U.S. customary units.

For D_{50} less than 0.03 m (0.1 ft) but greater than 0.0003 m (0.001 ft), Neill's critical velocity is given in equation 7.

$$V_{CN} = K_{U1} 11.5\, y_2^{x} D_{50}^{0.35} \tag{7}$$

The exponent, x, is calculated using equation 8:

$$x = K_{U2} \frac{0.123}{D_{50}^{0.20}} \tag{8}$$

where:

y_2 is equilibrium flow depth (m or ft).
D_{50} is sediment size (m or ft).
K_{U1} is, for SI units, 0.3048 to the power of 0.65 minus x, or 1.0 for U.S. customary units.
x is the exponent as calculated in equation 8.
K_{U2} is 0.788 for SI units, or 1.0 for U.S. customary units.

For D_{50} less than 0.0003 m (0.001 ft), Neill's critical velocity is given in equation 9.

$$V_{CN} = K_U \sqrt{y_2} \tag{9}$$

where:

y_2 is equilibrium flow depth (m or ft).
D_{50} is sediment size (m or ft).
K_U is 0.55217 for SI units, or 1.0 for U.S. customary units.

Chang's equations are plotted in figure 9. Neill's competent velocity curves are intended for field conditions with flow depths of 1.5 m (5 ft) or greater. Chang's equations were extrapolated to flow depths below 0.30 m for these experiments and to curves for flow depths of 0.305 and 0.15 m (1 and 0.5 ft) (see figure 9). Note that the sediment sizes used in the experiments fell into the range described by equations 7 and 8.

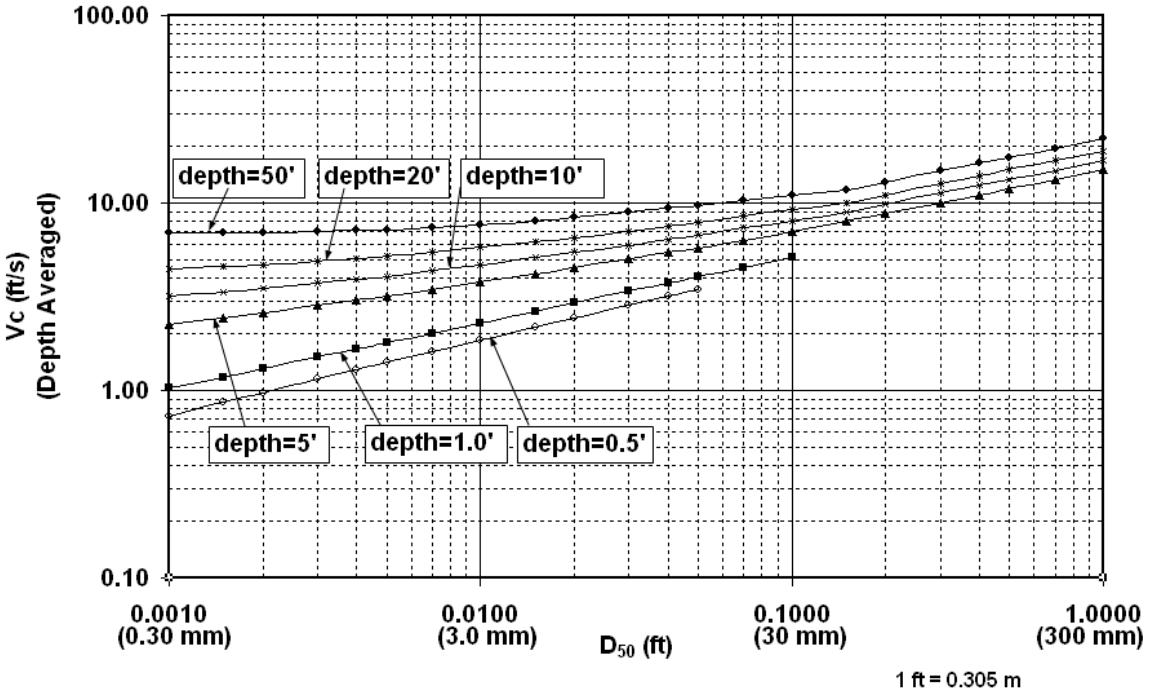

Figure 9. Graph. Chang's approximations to Neill's competent velocity curves.

Adjustment for Spiral Flow at Culvert Toe

This research revealed that the maximum scour depth, y_{max} (measured at the corners of the culvert), was always greater than the computed equilibrium depth, regardless of which equations for representative velocity and critical velocity were used. Thus, an empirical coefficient k_S, similar to an adjustment coefficient, was needed to explain the additional scour depth, as in the following equation:

$$\frac{y_{max}}{y_2} = k_S \tag{10}$$

Recalling from the discussion of equation 1 that y_2 equals q_R divided by V_C reveals that k_S will be a function of V_R and V_C, among other things. Our research considered two possibilities for a third independent parameter in the equation for k_S: the Froude number at the culvert approach, and a dimensionless ratio including $Q_{blocked}$ and y_2. $Q_{blocked}$ is the portion of the approach flow that is to one side of the channel centerline and that is blocked by the embankment as the flow approaches the culvert. Equations 11 and 12 give two different functions for k_S.

$$k_S = f_1(V_R, V_C, F_1) = f_1\left(V_R, V_C, \frac{Q}{y_1 w_a \sqrt{g\, y_1}}\right) \tag{11}$$

$$k_S = f_2(V_R, V_C, R_{Qblocked}) = f_2\left(V_R, V_C, \frac{Q_{blocked}}{\sqrt{g}\, y_2^{5/2}}\right) \tag{12}$$

Since there are three different expressions for V_R, two different expressions for V_c, and two different expressions for the third independent variable, this research considered 12 different k_S values.

Adjustment for Pressure Flow at a Submerged Culvert

The maximum scour depth, y_{max}, measured under submerged conditions, likewise was always greater than the computed equilibrium depth. Thus, an empirical coefficient, k_p, was needed to explain the additional scour depth, as in equation 13.

$$\frac{y_{max}}{y_2} = k_p k_S = f_3(A_k) f_{1,2}(V_R, V_C, F_1 \text{ or } R_{Qblocked}) \tag{13}$$

Equation 14 is the equation for A_k.

$$A_k = \frac{(y_1 - D) w_{CULV}}{w_a y_1} \tag{14}$$

where:

D is the culvert height at the approach prior to scour.
A_k is a dimensionless ratio: area of approaching flow directly above the culvert divided by the total area of flow approaching the culvert.

Note that due to the influence of k_S, this study will also consider 12 different values for k_p. Recall also that y_o in equation 1 for pressure flow is equal to the hydraulic grade line at the inlet (HGL_o in figure 8). These two different adjustment factors will be derived from experimental data for bottomless culverts in the results section.

SCOUR PROTECTION: RIPRAP ANALYSIS

Many researchers have developed critical conditions based on average velocity. Ishbash presented an equation that can be expressed as equation 15.[9]

$$N_{SC} = E \tag{15}$$

Ishbash described two critical conditions for riprap stability. For loose stones where no movement occurs, N_{SC} is expressed as equation 16.

$$N_{SC} = \frac{V_{min}^2}{[2g D_{50}(SG - 1)]} \tag{16}$$

$$E = 0.86$$

For loose stones allowed to roll until they become "seated," N_{SC} is expressed as equation 17.

$$N_{SC} = \frac{V_{\max}^{\ 2}}{[2g\,D_{50}(SG-1)]} \tag{17}$$

$$E = 1.44$$

where:

N_{SC}	is computed sediment number for distributed flow.
V_{min}	is minimum velocity (ft/s) that will remove the loose stones lying on top of the fill.
V_{max}	is maximum velocity (ft/s) that will roll out the stones lying among the others on the slope.
g	is acceleration of gravity (ft/s^2).
D_{50}	is diameter of riprap (ft).
SG	is specific gravity of riprap.
E	is the Ishbash constant.

Equation 17 for riprap that will just begin to roll can be written as equation 18. For the culvert experiments, we represented the effective velocity (V_{eff}) in terms of an empirical multiplier (equation 19) and the local bed velocity (equation 20), which is substituted into equation 17 to yield equation 21.

$$D_{50} = 0.69\,\frac{V_{eff}^{\ 2}}{2g\,(SG-1)} \tag{18}$$

$$V_{eff} = K_{RIP}\,V_{LB} \tag{19}$$

$$V_{LB} = K_{VM}\,V_{AC} \tag{20}$$

$$K_{RIP} = \frac{1.20\sqrt{2g\,(SG-1)\,D_{50}}}{V_{LB}} \tag{21}$$

where:

V_{eff}	is effective velocity that accounts for turbulence and vorticity in the mixing zone at the upstream corner of a culvert.
V_{LB}	is local velocity along the bed prior to scour in the vicinity of the upstream corner of a culvert.
V_{AC}	is average velocity in the contracted zone prior to scour in the vicinity of the upstream corner of a culvert.
K_{RIP}	is the coefficient used to size riprap for scour (to be determined in lab experiments).
K_{VM}	is the coefficient relating the local bed velocity in the experiments to the average velocity in the contraction zone (to be determined in lab experiments).

D_{50} is the diameter of riprap that is expected to be on the verge of failure in the vicinity of the upstream corner of the culvert.

Equations 18 through 21 are dimensionally homogeneous and can be used with either system of units as long as they are consistent.

4. RESULTS

The results presented in this section reflect the experiments described in the "Experimental Approach" section. The first subsection shows how these experiments compared with theoretical predictions of scour at the inlet of bottomless culverts. The second subsection presents scour maps that illustrate the scour that occurred at the culvert outlet. And the third subsection shows how the experiments relate to different scour countermeasures.

CLEAR WATER SCOUR EXPERIMENTS

This subsection presents the result of using laboratory experiments to determine the actual form of equations 4 and 11–13.

Representative Velocity

This section focuses on the calibration of V_{RM}. The representative velocities in the vicinity of the upstream corners of culverts were measured during fixed-bed experiments as prescour conditions. The measured V_{RM} values were then compared to the V_{RP} values from the potential flow theory to derive a multiplier, C, in equation 4, as illustrated in figure 10.

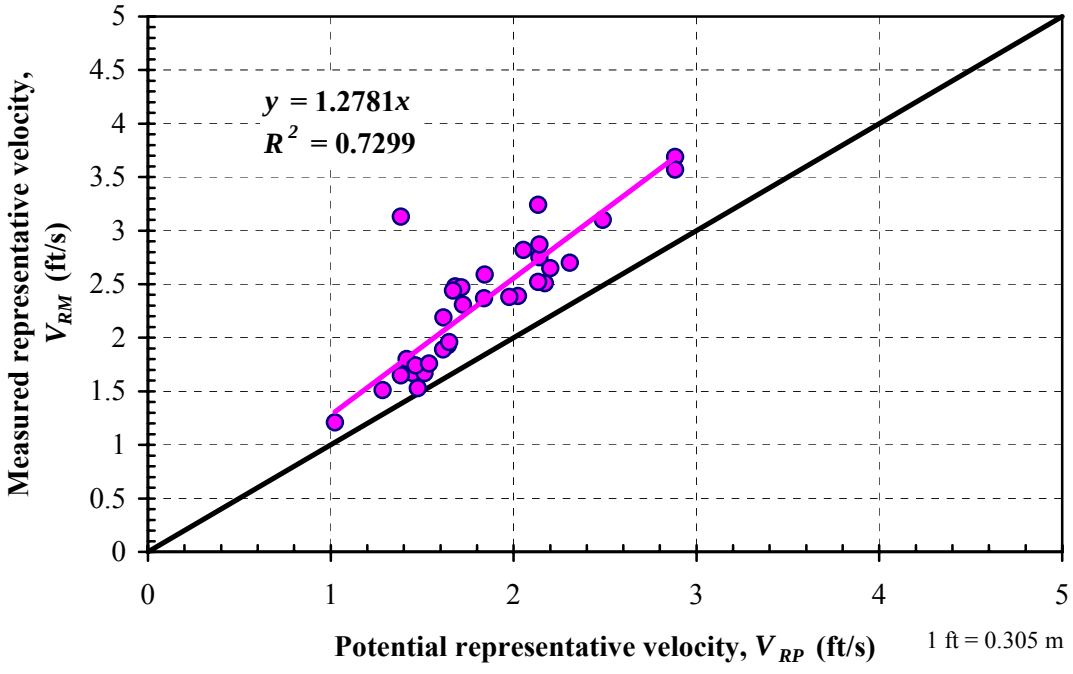

Figure 10. Graph. Calibration of *C* in equation 4.

A linear regression of the results shows that V_{RM} for bottomless culvert applications is 1.28 times V_{RP}. Thus, equation 4 can now be rewritten as equation 22.

$$V_{RM} = \left[1.024\left(\frac{q_1}{q_2}\right)^{1.5} + 1.28\right]\left[\frac{Q}{y_0 w_{CULV}}\right] \quad (22)$$

Spiral Flow Adjustment Factors

Experiments were used to determine the form of the 12 different expressions for k_S. Two examples are given.

The first example is the calibration and validation of k_S as a function of V_{RA}, V_{CL}, and the Froude number. In this combination, y_2 was calculated from equation 1 using the approach velocity, V_{RA} (equation 2), and Laursen's critical velocity, V_{CL} (equation 5). Figure 11 shows the regression of k_S versus the Froude number in the approach as the independent variable for bottomless culverts with and without wingwalls.

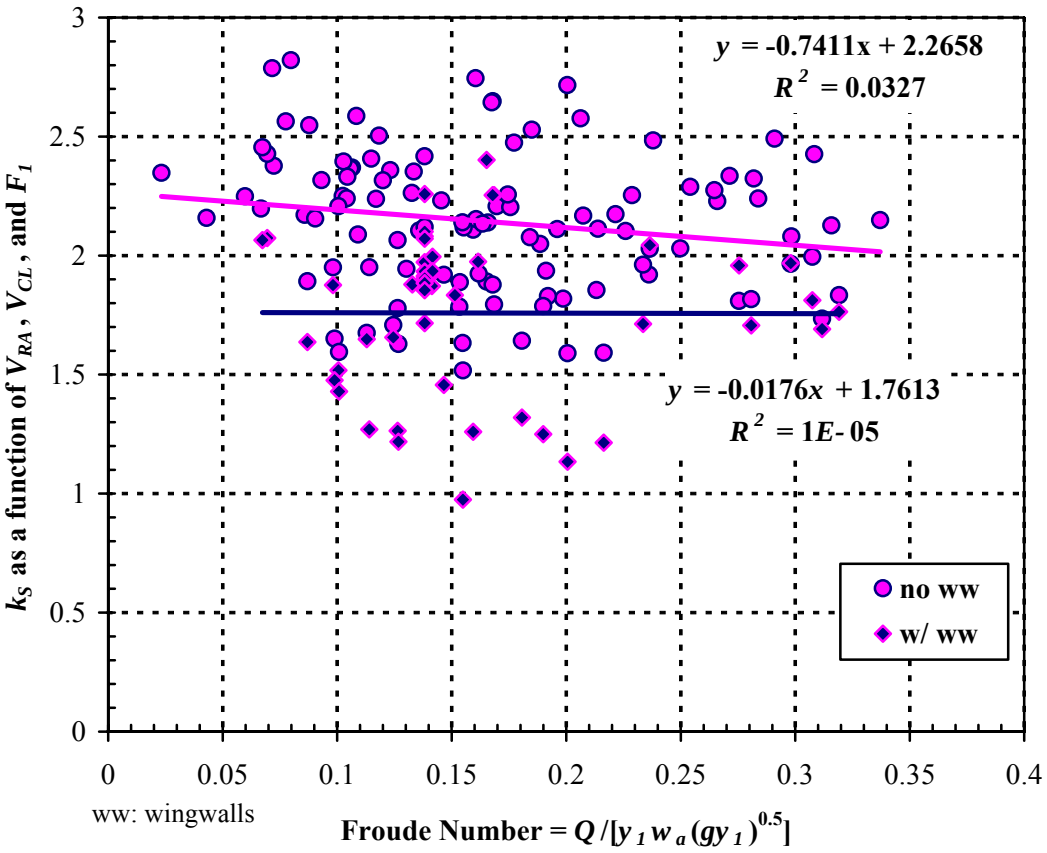

Figure 11. Graph. Calibration of k_S as a function of V_{RA}, V_{CL}, and F_1.

Figure 12 is a plot of y_{max} that was calculated using the regression equation from figure 11 versus the measured y_{max}.

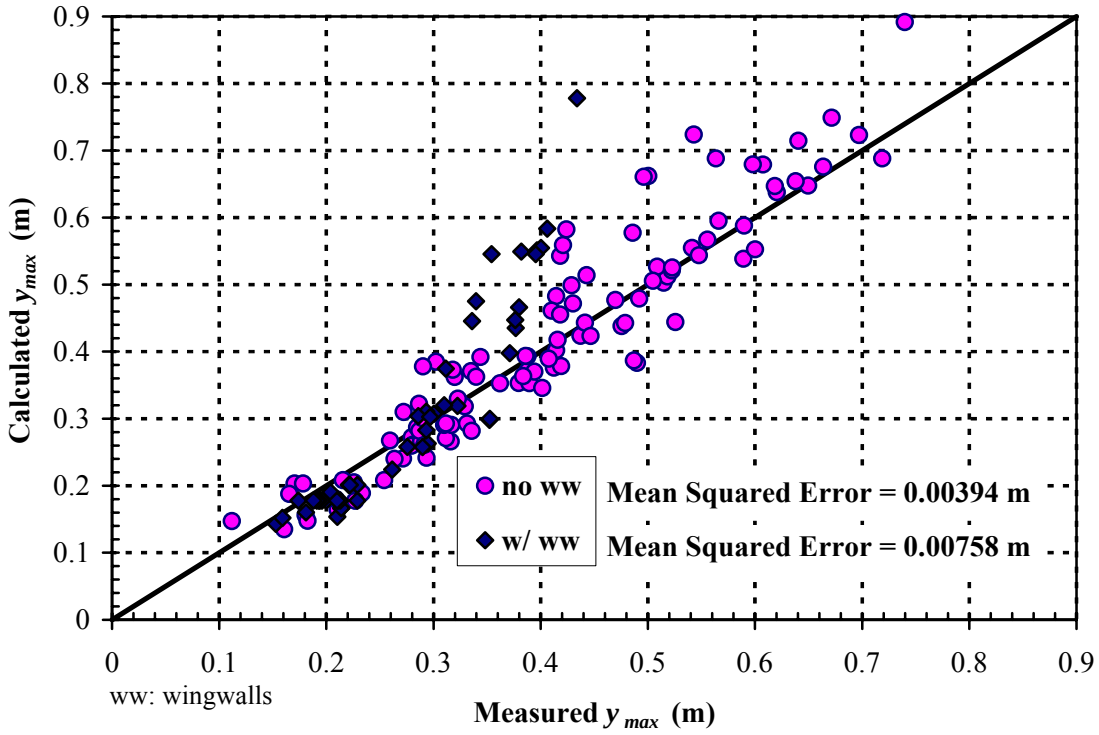

Figure 12. Graph. Validation of y_{max} using k_S as a function of V_{RA}, V_{CL}, and F_1.

The second example is the calibration and validation of k_S as a function of V_{RM}, V_{CN}, and the $Q_{blocked}$ ratio. In this combination, y_2 was calculated from equation 1 using the approach velocity, V_{RM} (equation 22), and Neill's critical velocity, V_{CN} (equations 7 and 8). Figure 13 shows the regression of k_S versus the $Q_{blocked}$ ratio as the independent variable for bottomless culverts with and without wingwalls.

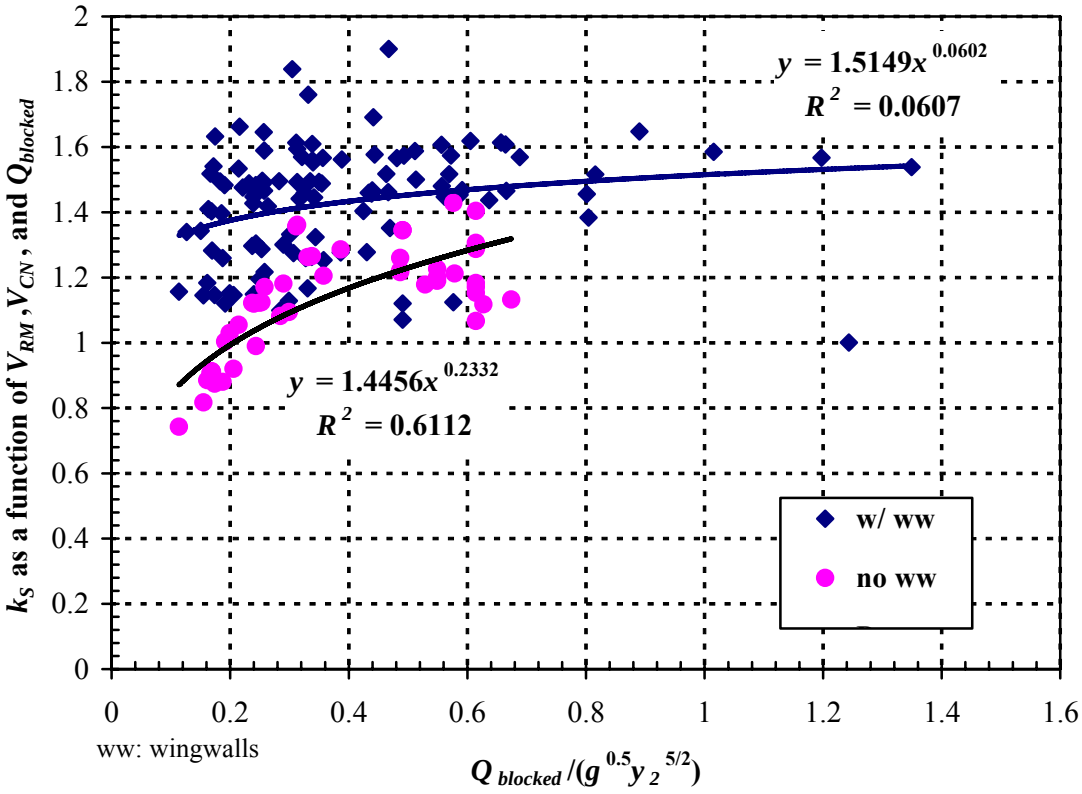

Figure 13. Graph. Calibration of k_S as a function of V_{RM}, V_{CN}, and $Q_{blocked}$.

Figure 14 is a plot of y_{max} that was calculated using the regression equation from figure 13 versus the measured y_{max}.

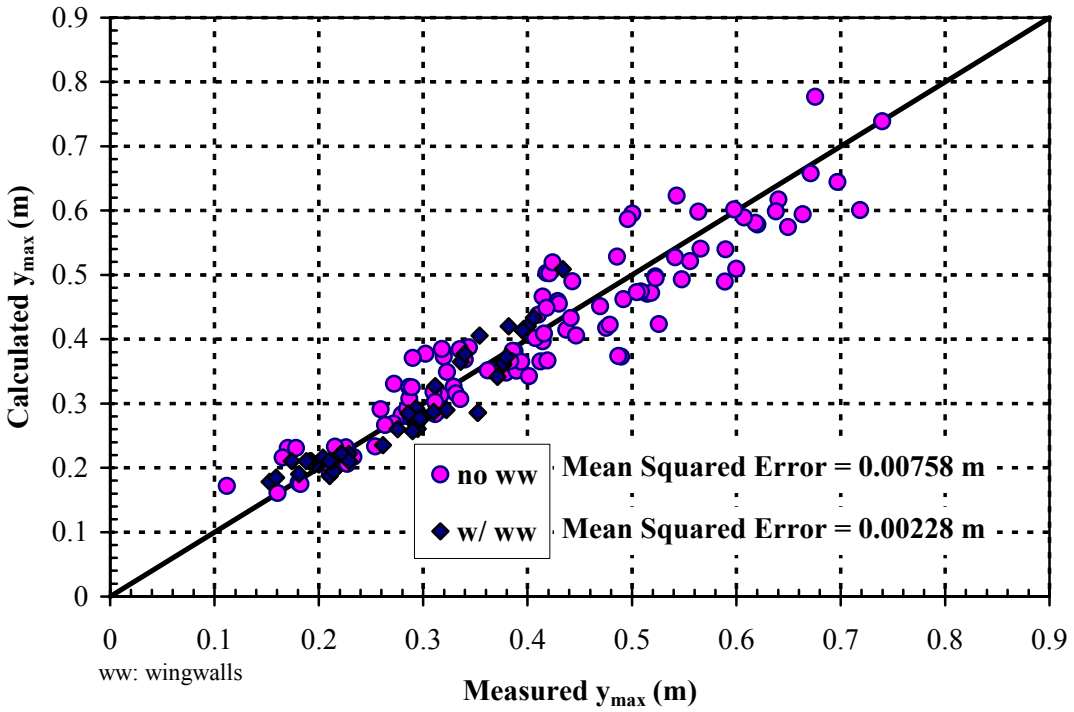

Figure 14. Graph. Validation of y_{max} using k_S as a function of V_{RM}, V_{CN}, and $Q_{blocked}$.

Similar calculations and plots were obtained for the other ten k_S combinations. Table 2 summarizes the scour equation for each scenario for unsubmerged bottomless culverts, and some calibration and validation statistics. The Froude numbers in the experiments did not cover the full range that is expected in the field, and the negative slopes presented in table 2 are probably not realistic. For this reason, we recommend changing the Froude number multiplier to zero for equations in table 2 with negative slopes.

Table 2. Unsubmerged scour equations.

Equation 1 Parameters	Unsubmerged Scour Equation	Calibration R^2	Validation (Mean Error)^2 (m)
$y_2 = f(V_{RA}, V_{CL})$	$no\ ww: \quad k_S = (-0.7411 F_1 + 2.2658)$	0.0327	0.00394
	$w/ww: \quad k_S = (-0.0176 F_1 + 1.7613)$	0.00001	0.00758
$y_2 = f(V_{RA}, V_{CL})$	$no\ ww: \quad k_S = (2.1389 R_{Qblocked}^{0.1197})$	0.2948	0.0148
	$w/ww: \quad k_S = (1.7273 R_{Qblocked}^{0.2779})$	0.7764	0.00460
$y_2 = f(V_{RA}, V_{CN})$	$no\ ww: \quad k_S = (-0.956 F_1 + 2.0758)$	0.0834	0.00394
	$w/ww: \quad k_S = (-0.0456 F_1 + 1.5235)$	0.0002	0.00758
$y_2 = f(V_{RA}, V_{CN})$	$no\ ww: \quad k_S = (1.9458 R_{Qblocked}^{0.0693})$	0.0799	0.00402
	$w/ww: \quad k_S = (1.63 R_{Qblocked}^{0.2345})$	0.6251	0.000838
$y_2 = f(V_{RP}, V_{CL})$	$no\ ww: \quad k_S = (-0.6555 F_1 + 2.0041)$	0.0327	0.00394
	$w/ww: \quad k_S = (-0.0155 F_1 + 1.5579)$	0.00001	0.00758
$y_2 = f(V_{RP}, V_{CL})$	$no\ ww: \quad k_S = (1.5883 R_{Qblocked}^{0.1197})$	0.2948	0.00916
	$w/ww: \quad k_S = (1.3465 R_{Qblocked}^{0.2779})$	0.7764	0.00361
$y_2 = f(V_{RP}, V_{CN})$	$no\ ww: \quad k_S = (-0.8538 F_1 + 1.8643)$	0.0837	0.00284
	$w/ww: \quad k_S = (-0.031 F_1 + 1.3696)$	0.0001	0.00365
$y_2 = f(V_{RP}, V_{CN})$	$no\ ww: \quad k_S = (1.7777 R_{Qblocked}^{0.066})$	0.0726	0.00231
	$w/ww: \quad k_S = (1.56 R_{Qblocked}^{0.234})$	0.62	0.00754
$y_2 = f(V_{RM}, V_{CL})$	$no\ ww: \quad k_S = (-0.5305 F_1 + 1.6219)$	0.0327	0.00394
	$w/ww: \quad k_S = (-0.0126 F_1 + 1.2608)$	0.00001	0.00781
$y_2 = f(V_{RM}, V_{CL})$	$no\ ww: \quad k_S = (1.6921 R_{Qblocked}^{0.1197})$	0.2948	0.00916
	$w/ww: \quad k_S = (1.5597 R_{Qblocked}^{0.2779})$	0.7764	0.00361
$y_2 = f(V_{RM}, V_{CN})$	$no\ ww: \quad k_S = (-0.7025 F_1 + 1.5491)$	0.0842	0.00239
	$w/ww: \quad k_S = (-0.0114 F_1 + 1.1399)$	0.00002	0.00359
$y_2 = f(V_{RM}, V_{CN})$	$no\ ww: \quad k_S = (1.5149 R_{Qblocked}^{0.0602})$	0.0607	0.00228
	$w/ww: \quad k_S = (1.4456 R_{Qblocked}^{0.2332})$	0.6112	0.00758

Note: As discussed in the text, the Froude number multiplier should be changed to zero for equations with negative slopes.

Pressure Flow Adjustment Factors

Although future experiments eventually will expand the range of the submerged flow conditions presented here, this section shows preliminary results for scour in a submerged bottomless culvert. These preliminary experiments were also used to determine the form

of the 12 different expressions for k_p that correspond to the 12 different k_S equations in the previous section. Recall also that y_0 in equation 1 for pressure flow is equal to the hydraulic grade line at the inlet (HGL_o in figure 8). Two examples, similar to the k_S section, are given.

The first example is the calibration and validation of k_p as a function of A_k when k_S is a function of V_{RA}, V_{CL}, and F_1 (equations 13 and 14). In this combination, y_2 was calculated from equation 1 using the approach velocity, V_{RA} (equation 2), and Laursen's critical velocity, V_{CL} (equation 5). Figure 15 shows the regression of k_p versus A_k as the independent variable for bottomless culverts with wingwalls.

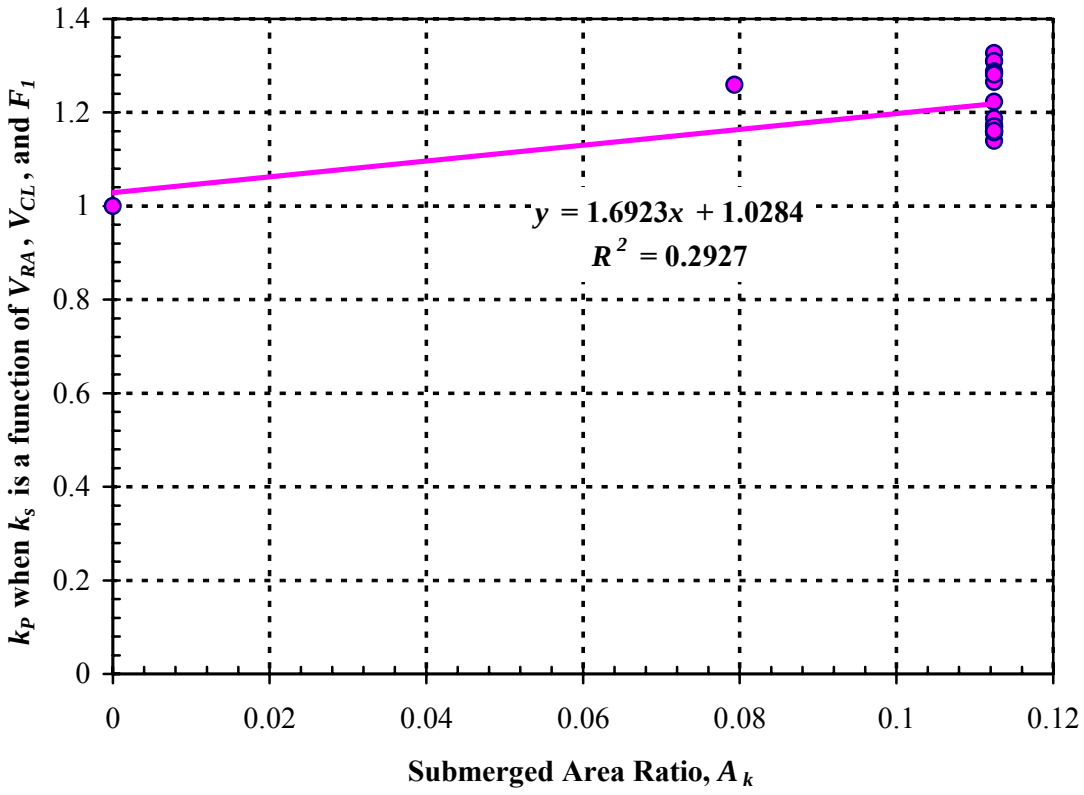

Figure 15. Graph. Calibration of k_p when k_s is a function of V_{RA}, V_{CL}, and F_1.

Figure 16 is a plot of y_{max} that was calculated using the regression equation from figure 15 versus the measured y_{max}.

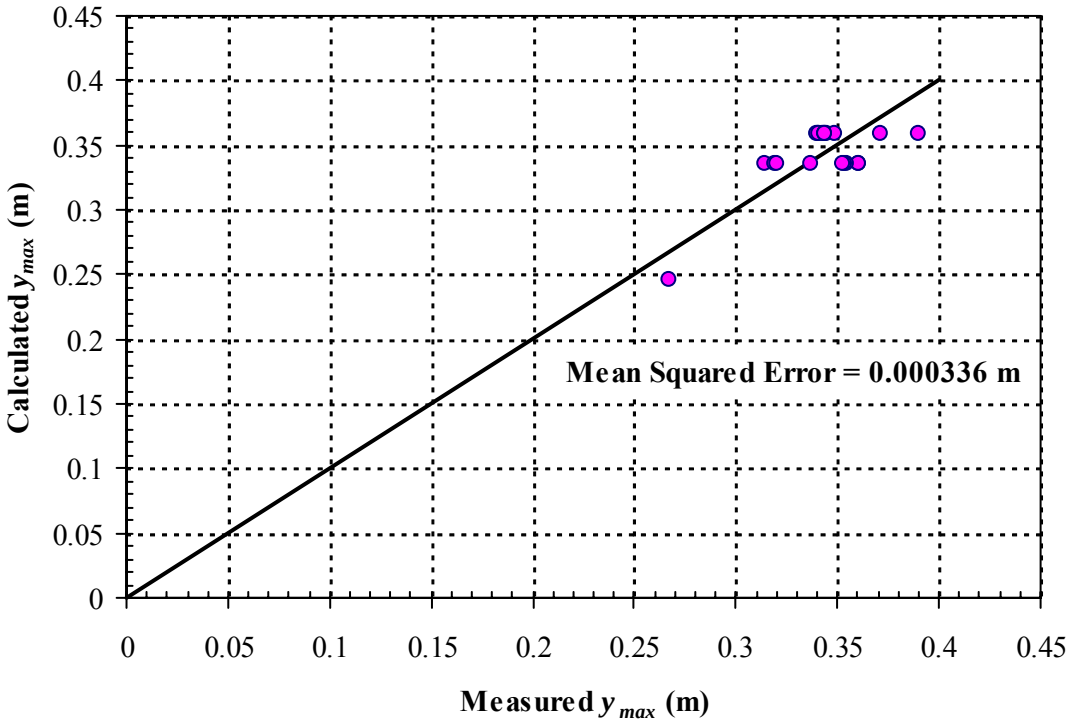

Figure 16. Graph. Validation of y_{max} using k_p when k_s is a function of V_{RA}, V_{CL}, and F_1.

The second example is the calibration and validation of k_p as a function of A_k when k_s is a function of V_{RM}, V_{CN}, and $Q_{blocked}$ (equations 13 and 14). In this combination, y_2 was calculated from equation 1 using the approach velocity, V_{RM} (equation 22), and Neill's critical velocity, V_{CN} (equations 7 and 8). Figure 17 shows the regression of k_p versus A_k as the independent variable for bottomless culverts with wingwalls.

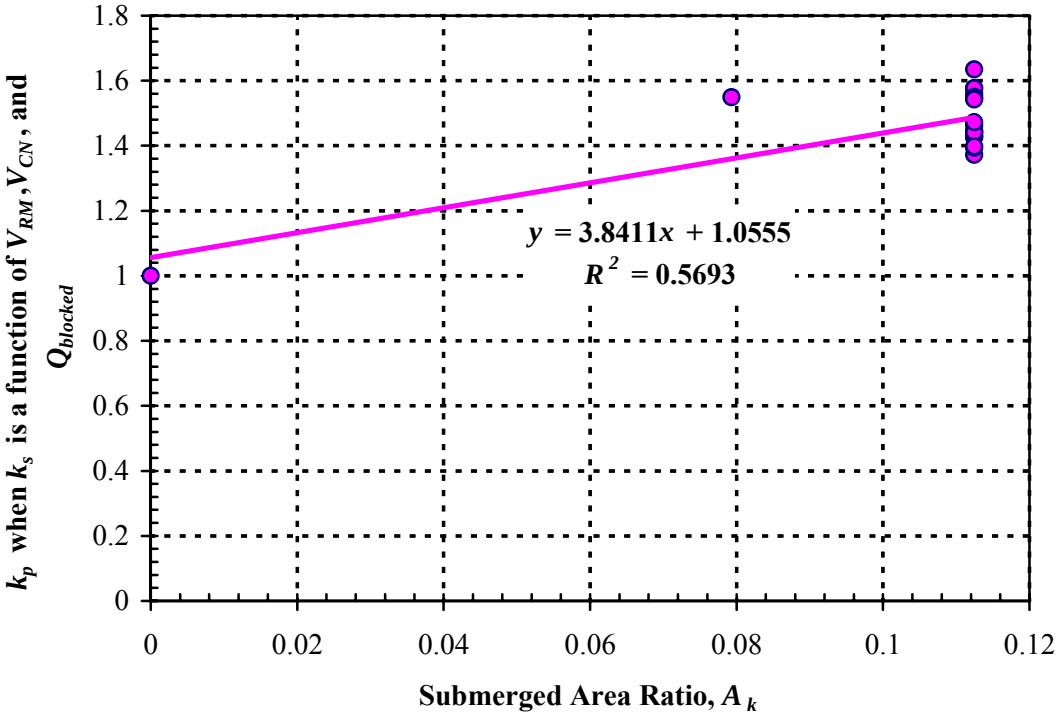

Figure 17. Graph. Calibration of k_p when k_s is a function of V_{RM}, V_{CN}, and $Q_{blocked}$.

Figure 18 is a plot of y_{max} that was calculated using the regression equation from figure 17 versus the measured y_{max}.

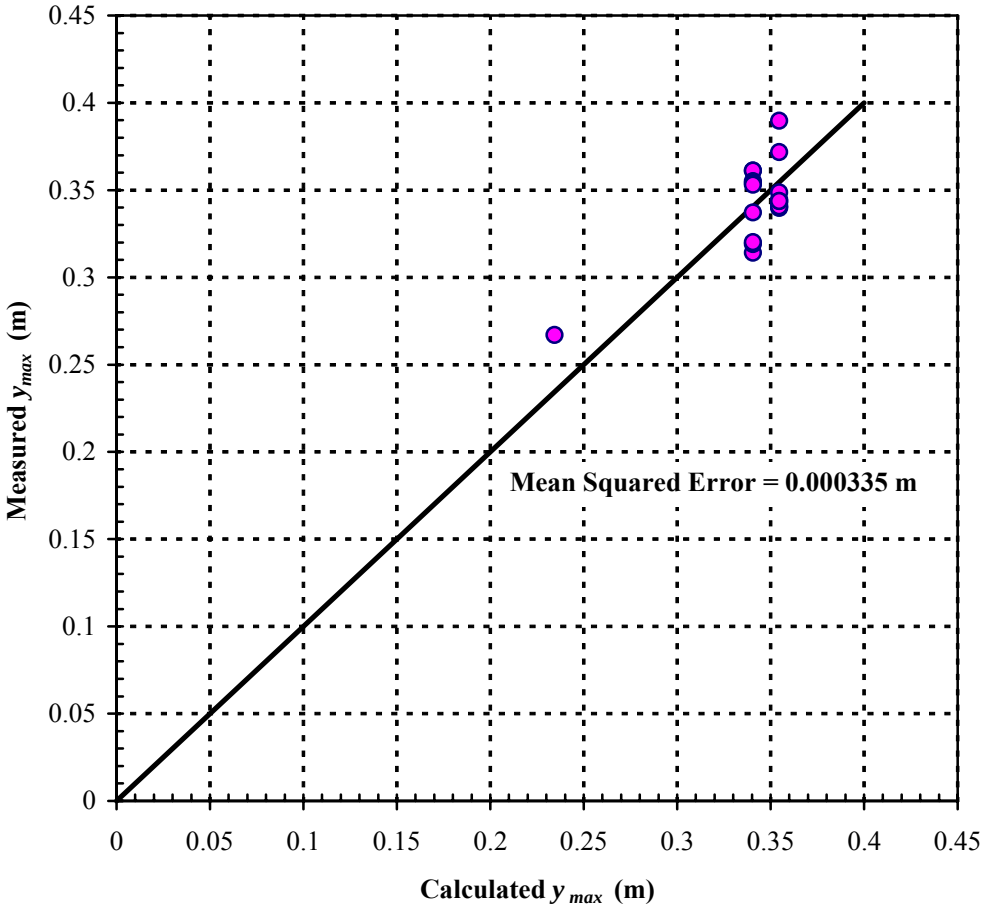

Figure 18. Graph. Validation of y_{max} using k_p when k_s is a function of V_{RM}, V_{CN}, and $Q_{blocked}$.

All of the k_p equations derived in the preceding discussion can be substituted into equation 13 to obtain equations for the maximum scour depth in a submerged bottomless culvert. Table 3 summarizes the scour equation for each scenario. The Froude numbers in the experiments did not cover the full range that is expected in the field, and the negative slopes presented in table 3 are probably not realistic. For this reason, we recommend changing the Froude number multiplier to zero for equations in table 3 with negative slopes.

Table 3. Submerged scour equations for culverts with wingwalls.

Equation 1 Parameters	Submerged Scour Equation	Calibration R^2 / (Mean Error)^2
$y_2 = f(V_{RA}, V_{CL})$	$k_p = (-0.0176 F_1 + 1.7613)(1.6923 A_k + 1.0284)$	0.2927 0.000336 m
$y_2 = f(V_{RA}, V_{CL})$	$k_p = (1.7273 R_{Qblocked}^{0.2779})(4.2862 A_k + 1.0737)$	0.5653 0.00539 m
$y_2 = f(V_{RA}, V_{CN})$	$k_p = (-0.0456 F_1 + 1.5235)(2.0225 A_k + 1.0183)$	0.3896 0.000307 m
$y_2 = f(V_{RA}, V_{CN})$	$k_p = (1.63 R_{Qblocked}^{0.2345})(3.1353 A_k + 1.0481)$	0.5092 0.00149 m
$y_2 = f(V_{RP}, V_{CL})$	$k_p = (-0.0155 F_1 + 1.5579)(1.6923 A_k + 1.0284)$	0.2927 0.000336 m
$y_2 = f(V_{RP}, V_{CL})$	$k_p = (1.3465 R_{Qblocked}^{0.2779})(4.0963 A_k + 1.0714)$	0.5536 0.00456 m
$y_2 = f(V_{RP}, V_{CN})$	$k_p = (-0.031 F_1 + 1.3696)(2.0082 A_k + 1.0182)$	0.3869 0.000307 m
$y_2 = f(V_{RP}, V_{CN})$	$k_p = (1.56 R_{Qblocked}^{0.234})(2.6483 A_k + 1.0427)$	0.4554 0.00146 m
$y_2 = f(V_{RM}, V_{CL})$	$k_p = (-0.0126 F_1 + 1.2608)(1.6923 A_k + 1.0284)$	0.2927 0.000336 m
$y_2 = f(V_{RM}, V_{CL})$	$k_p = (1.5597 R_{Qblocked}^{0.2779})(3.7757 A_k + 1.0676)$	0.5316 0.00417 m
$y_2 = f(V_{RM}, V_{CN})$	$k_p = (-0.0114 F_1 + 1.1399)(1.9836 A_k + 1.018)$	0.3823 0.000307 m
$y_2 = f(V_{RM}, V_{CN})$	$k_p = (1.4456 R_{Qblocked}^{0.2332})(3.8411 A_k + 1.0555)$	0.5693 0.000335 m

Note: As discussed in the text, the Froude number multiplier should be changed to zero for equations with negative slopes.

OUTLET SCOUR EXPERIMENTS

The bottomless culvert outlet scour experiments were completed in accordance with the test matrix (table 1). Specifically, the following results are presented and discussed:

- Fixed-bed prescour conditions, including velocity distributions analyzed using particle image velocimetry (PIV), for rectangular culverts with 45-degree wingwalls.
- Submerged entrance conditions for both fixed and movable bed conditions.
- Effects of various inlet and outlet wingwall configurations on resulting scour patterns (including location, lateral extent, and maximum depth of scour).
- Preliminary test of pile dissipator design to reduce outlet scour.

- Effectiveness of MDSHA Standard Plan to reduce scour.

- Revised stability coefficients and regression equations for sizing and placing riprap at entrances to bottomless culverts (originally presented in Phase I of this study) (discussed in a separate section).

- Performance of Rosgen-type cross vanes near bottomless culvert entrances, in the approach flow, as countermeasures to reduce culvert scour and channel instability (discussed in a separate section).

A sample of the resulting scour maps is given in appendix A. A table that summarizes the parameters for each experiment in appendix A is given in appendix B.

Flow Conditions

Fixed Bed

Fixed-bed tests were conducted to measure prescour conditions, which are the conditions best suited for the methodology proposed in Phase I to predict scour (figure 19). Detailed velocity distributions were measured at the culvert entrance using advanced techniques. A display of velocity distributions is provided in figure 20.

Figure 19. Photo. Outlet prior to scour test.

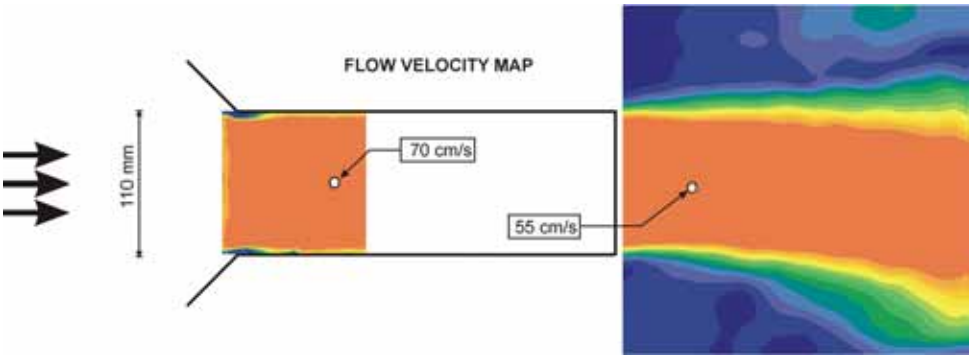

Figure 20. Image. Velocity distribution for unsubmerged culvert with 45-degree wingwalls at entrance.

From the fixed-bed experiments, it is clear that the vorticity increases as flow moves away from the culvert exit. The turbulent shear stress map in figure 21 shows very high shear stress at two locations a distance beyond the culvert outlet. These high shear stresses explain why scour holes are created in a moveable bed (figure 22). As shown in figure 23, adding wingwalls at the outlet reduces the shear stress, and thus reduces the outlet (downstream) scour hole depth (figure 24).

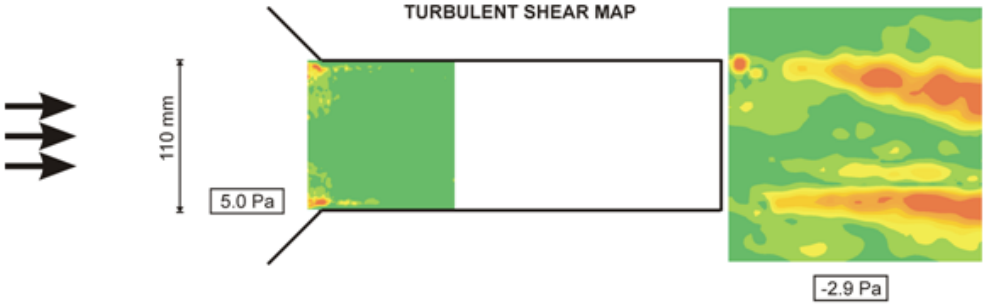

Figure 21. Image. Turbulent shear map for outlet with no wingwalls.

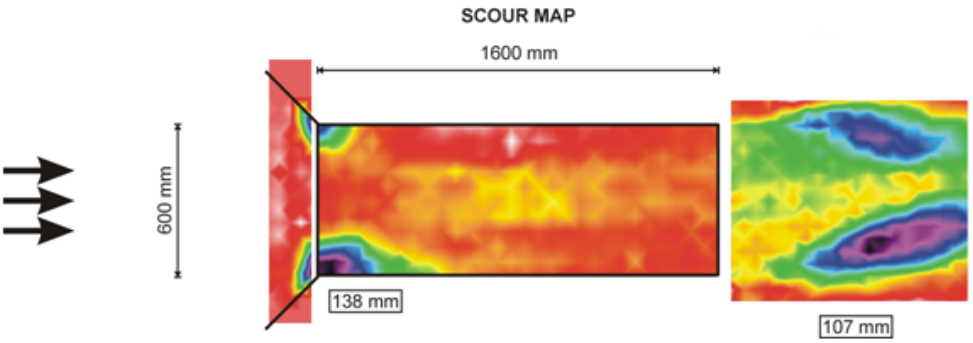

Figure 22. Image. Scour map for outlet with no wingwalls.

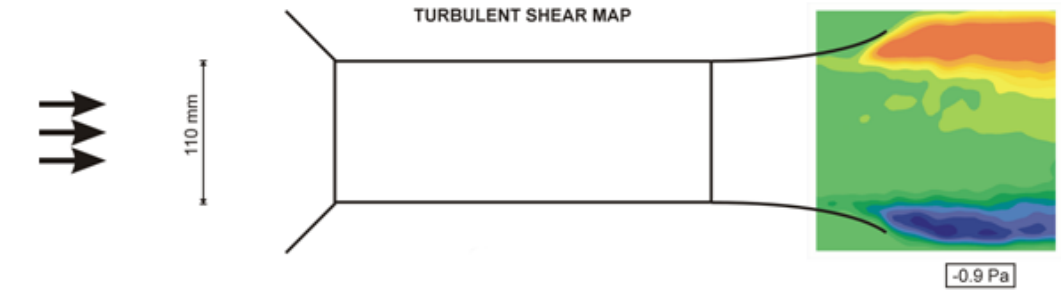

Figure 23. Image. Turbulent shear map for outlet with streamlined wingwalls.

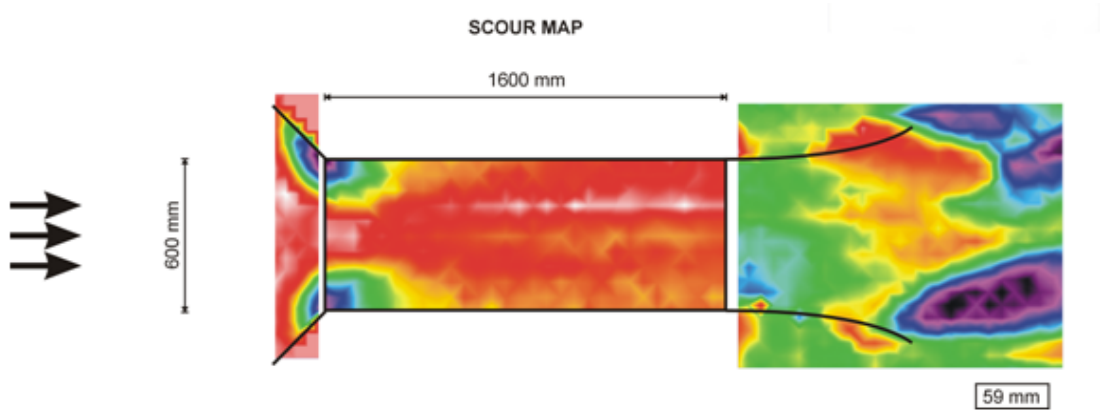

Figure 24. Image. Scour map for outlet with streamlined wingwalls.

Movable Bed

Movable bed tests were conducted to measure scour conditions at the outlet for a variety of wingwall configurations (figure 25).

Figure 25. Photo. Outlet scour after test.

Submerged and Unsubmerged Conditions

Various inlet and outlet wingwall configurations were investigated under both submerged and unsubmerged flow conditions to determine the overall effects of the flow conditions on scour hole formation. The results show that submerged flow conditions induce greater inlet scour depths, while unsubmerged flow conditions induce greater outlet scour depths.

Wingwalls

Wingwalls have traditionally been constructed with highway culverts to increase flow capacity (for culverts operating in inlet control) and reduce the severity of erosion and scour of both the channel and adjacent banks at both the inlet and outlet. Various inlet and outlet wingwall configurations were investigated under both submerged and unsubmerged flow conditions to determine the overall effects of wall shape, length, and orientation on scour hole formation. The results from the experimental wingwall studies are covered in the following paragraphs. Maps for all of the resulting scour profiles can be found in appendix A.

Inlet Wingwalls

While the study focused on outlet scour, inlet wingwalls and their impacts on the scour at the inlet were also investigated. The experimental culvert setup was used to model a square culvert inlet with and without wingwalls for both submerged and unsubmerged flow conditions. Wingwalls were built with a 45-degree and an 8-degree flare. As demonstrated by the inlet experiments, upstream scour is deeper in submerged, pressure flow conditions. The results also show that 45-degree inlet wingwalls are effective at reducing inlet scour, whereas 8-degree inlet wingwalls are not effective. See table 4 and related figures 26 through 29.

Table 4. Inlet wingwall test configurations.

Inlet Wingwall Type	Experiment Photos	Submerged/ Unsubmerged	Representative Inlet Scour Map (see Appendix A)
45-degree flare	Figures 26, 27	Submerged	Figure 62
		Unsubmerged	Figure 63
8-degree flare (smooth joint)	Figures 28, 29	Submerged	Figure 71
		Unsubmerged	Figure 70

Figure 26. Photo. 45-degree inlet wingwalls before scour.

Figure 27. Photo. 45-degree inlet wingwalls after scour.

Figure 28. Photo. 8-degree inlet wingwalls before scour.

Figure 29. Photo. 8-degree inlet wingwalls after scour.

Outlet Wingwalls

As demonstrated by the outlet experiments, downstream scour is deeper in unsubmerged conditions (table 5). However, scour in unsubmerged conditions can be substantially reduced by the use of outlet wingwalls with a streamlined shape (compare figures referenced in table 5). Experimental results indicate that turbulence is reduced and "vortex shedding" caused by abrupt changes in pressure is almost eliminated by use of

this shape. In other words, the streamlined wall eliminates flow separation and decreases turbulence.[10] Hence, with the streamlined bevel, vortices do not propagate downstream and the resulting turbulence is more evenly distributed—not concentrated in a single location. Conversely, the abrupt change in pressure that results from a square exit shape (as found in culverts without wingwalls at the outlet) induces vortex shedding and increased scour depths.

Table 5. Outlet wingwall test configurations.

Outlet Wingwall Type	Experiment Photos	Representative Outlet Scour Map(see Appendix A)
No wingwall	Figure 30	Figure 63
Truncated, circular	Figures 31, 32	Figure 64
Elongated, streamlined	Figures 33, 34	Figure 65
Short bevel	Figure 35	Figure 66
8-degree flare (rough joint)	Figures 36, 37	Figure 68
8-degree flare (smooth joint)	Figures 38, 39	Figure 69
45-degree flare	Figure 40	Figure 67

Figure 30. Photo. No wingwalls.

Figure 31. Photo. Truncated, circular wingwalls before scour.

Figure 32. Photo. Truncated, circular wingwalls after scour.

Figure 33. Photo. Elongated, streamlined wingwalls before scour.

Figure 34. Photo. Elongated, streamlined wingwalls after scour.

Figure 35. Photo. Short, streamlined bevel wingwalls after scour.

Figure 36. Photo. Wingwalls with 8-degree flare (rough joint) before scour.

Figure 37. Photo. Wingwalls with 8-degree flare (rough joint) after scour.

Figure 38. Photo. Wingwalls with 8-degree flare (smooth joint) before scour.

Figure 39. Photo. Wingwalls with 8-degree flare (smooth joint) after scour.

Figure 40. Photo. 45-degree wingwalls after scour.

Scour Countermeasures

Four scour countermeasures were evaluated other than wingwalls: riprap, cross vanes, pile dissipators at the outlet, and the MDSHA Standard Plan combination of countermeasures. The results of the riprap and cross vane analyses are presented later in this report.

Outlet Scour Control Using Pile Dissipators

Chang at MDSHA designed a series of group piles herein called pile dissipators (cylindrical pegs, 25 mm (0.975 inch) in diameter and 12 cm (4.68 inches) in height, mounted on a board) to reduce scour at the culvert outlet.[(2)] Table 6 lists the three tests used to evaluate this type of countermeasure, and the scour maps presented in appendix A that illustrate their effect. Figure 41 shows a photo of the pile dissipators used in the experiments, and figure 42 shows the position of the dissipators. Figure 43 shows the culvert prior to scour, while the last two photos show the resultant scour both without (figure 44) and with (figure 45) pile dissipators. The maximum scour depth without pile dissipators was 110 mm (4.29 inches), while the scour with dissipators ranged from 84 to 91 mm (3.28 to 3.55 inches). In other words, the pile dissipators decreased the scour depth by 17 to 26 percent.

Table 6. Tests using pile dissipators.

Inlet/Outlet Wingwall Type	Submerged/ Unsubmerged	Representative Outlet Scour Map (see Appendix A)
Inlet/outlet walls with 45-degree flare; pile dissipators not used	Submerged	Figure 72
Inlet/outlet walls with 45-degree flare; pile dissipators used	Submerged	Figure 73

Figure 41. Photo. Pile dissipators.

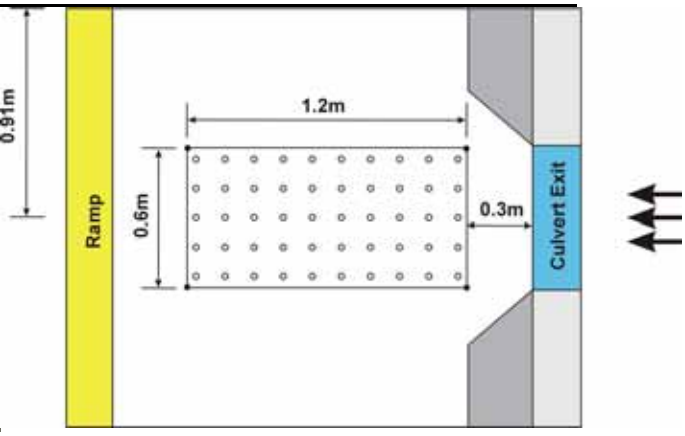

Figure 42. Diagram. Plan view of pile dissipators.

Figure 43. Photo. Culvert outlet prior to pile dissipator test.

Figure 44. Photo. Outlet scour area without protective pile dissipators.

Figure 45. Photo. Outlet scour area with protective pile dissipators.

Scour Control Using MDSHA Standard Plan Methods

The MDSHA Standard Plan was tested as a scour countermeasure design. This design employs wingwalls at the inlet and outlet of the culvert and lines the wingwalls and the inside walls of the culvert with riprap (D_{50} equals 25 mm (0.975 inches); see figures 46 and 47). The plan was tested under submerged conditions with 45-degree inlet wingwalls and both 45-degree and streamlined beveled outlet wingwalls. Figures 48 to 50 show the tests prior to scour with the riprap positioned along the corners of the culvert. The plan was tested with a flow depth of 23 cm (8.97 inches) and a velocity of 13 cm/s (5.07 inches/s). When the plan was tested, the riprap moved and fell into the scour holes, after which the riprap stabilized (figures 51 and 52). Table 7 shows the results. Since these results are still preliminary, this report does not make any recommendations about sizing or placing riprap for this design.

Table 7. Tests using MDSHA Standard Plan methods.

Inlet/Outlet Wingwall Type	Submerged/ Unsubmerged	Representative Outlet Scour Map (see Appendix A)
Inlet/outlet walls with 45-degree flare	Submerged	Figure 74

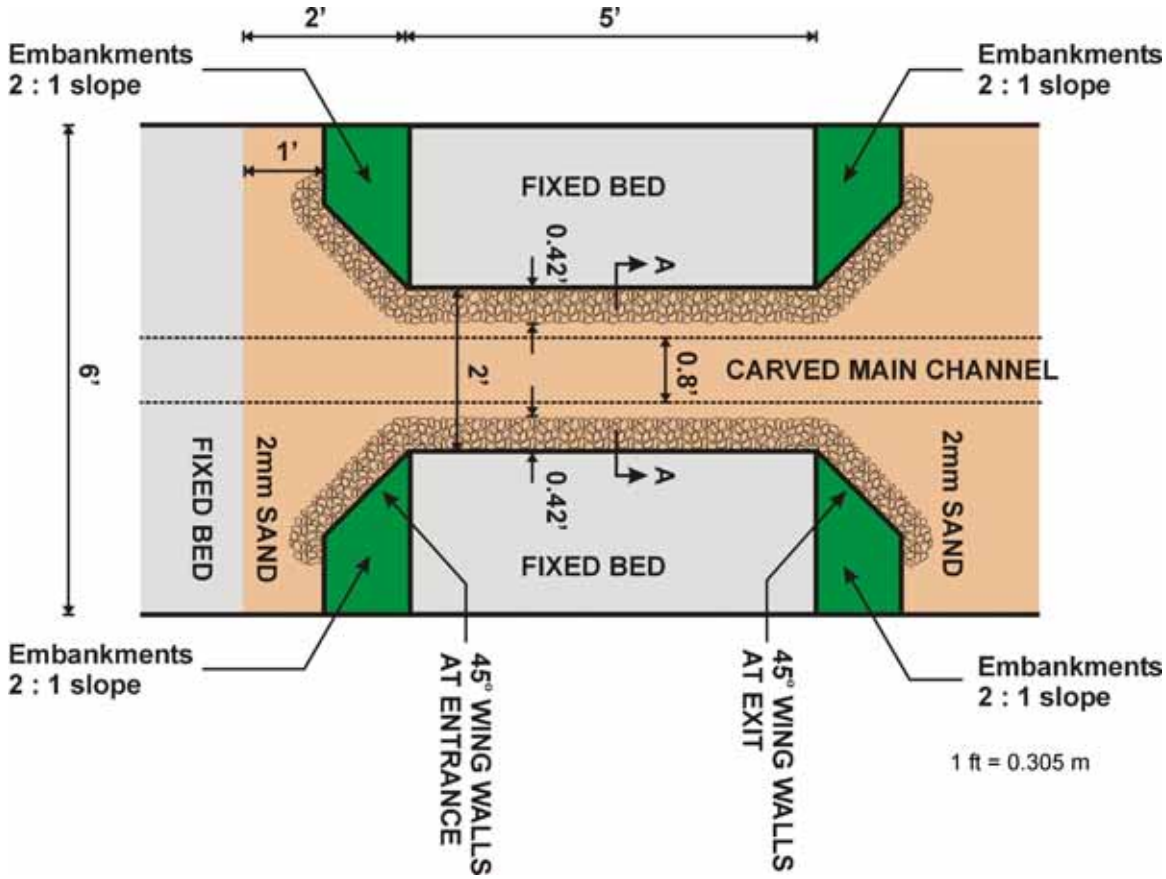

Figure 46. Diagram. Countermeasure installation for MDSHA Standard Plan (top view).

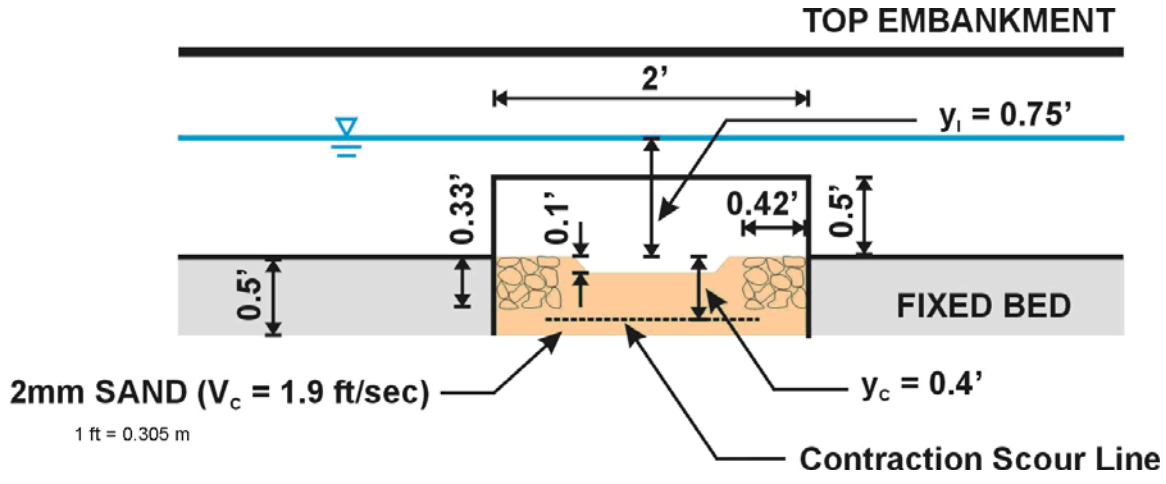

Figure 47. Diagram. Countermeasure installation for MDSHA Standard Plan (Section A-A from figure 46).

Figure 48. Photo. Culvert inlet before Standard Plan test.

Figure 49. Photo. Culvert barrel before Standard Plan test.

Figure 50. Photo. Culvert outlet before Standard Plan test.

Figure 51. Photo. Shifted riprap in culvert inlet after Standard Plan test.

Figure 52. Photo. Shifted riprap in culvert barrel after Standard Plan test.

RIPRAP STABILITY DESIGN COEFFICIENTS

The data collected were the local bed velocity (V_{LB}) and the average contraction velocity (V_{AC}), the ratio of which is plotted versus the Froude number in the contraction zone in figure 53.

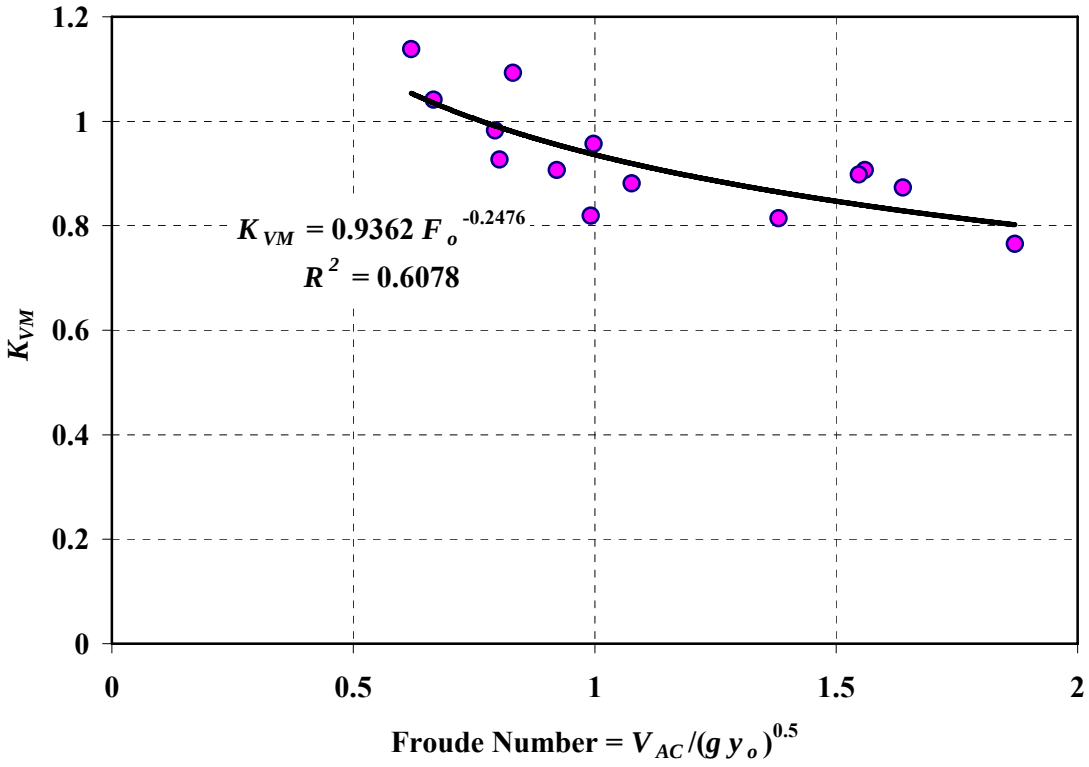

Figure 53. Graph. Calibrated function for K_{VM}.

Figure 53 reveals that the equation for K_{VM} takes the form of equation 23.

$$K_{VM} = \frac{V_{LB}}{V_{AC}} = 0.94F_o^{-0.25} \quad (23)$$

Data collected for different riprap sizes (for which V_{eff} was calculated using equation 19) by measuring the local velocity prior to movement were used to calibrate K_{RIP}, which is plotted versus the Froude Number at the contraction in figure 54.

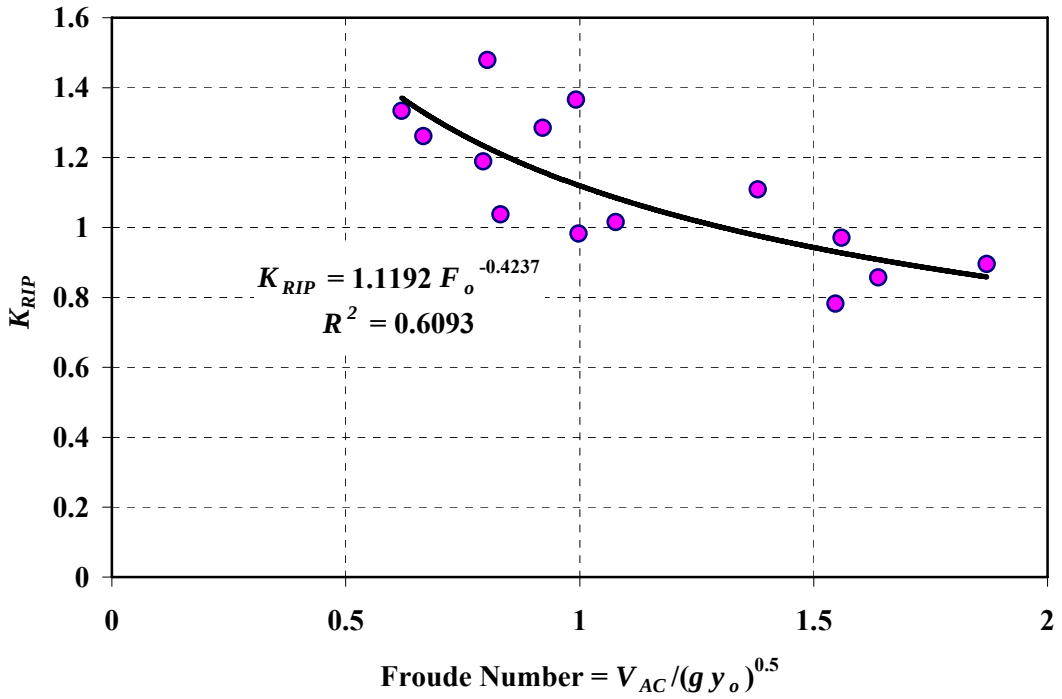

Figure 54. Graph. Calibration function for K_{RIP}.

The fitted relationship in figure 54 reveals that the equation for K_{RIP} takes the form of equation 24.

$$K_{RIP} = \frac{V_{eff}}{V_{LB}} = 1.12 F_o^{-0.42} \tag{24}$$

Rewriting equation 17 by inserting equations 18 and 19 in terms of D_{50} produces equation 25.

$$D_{50} = 0.69 \frac{V_{eff}^2}{2g(SG-1)} = 0.69 \frac{(K_{RIP} V_{LB})^2}{2g(SG-1)} = 0.69 \frac{(K_{RIP} K_{VM} V_{AC})^2}{2g(SG-1)} \tag{25}$$

Substituting equations 23 and 24, dividing both sides by y_o, and collecting similar terms yields equation 26.

$$\frac{D_{50}}{y_o} = \frac{0.69(1.12 F_o^{-0.42}\ 0.94 F_o^{-0.25})^2}{2(SG-1)} \frac{(V_{AC})^2}{g\ y_o} = \frac{0.76 F_o^{-1.34}}{2(SG-1)} F_o^2 \tag{26}$$

Thus, the final dimensionless equation calculating D_{50} from y_o and F_o is equation 27.

$$\frac{D_{50}}{y_o} = \frac{0.38 F_o^{0.66}}{SG-1} = \frac{0.38}{SG-1} \left(\frac{V_{AC}^2}{g\ y_o} \right)^{0.33} \tag{27}$$

To validate the results, V_{AC} measurements and Froude number measurements were used to calculate the design D_{50} using equation 27. Figure 55 shows that the calculated D_{50} matches the D_{50} of the riprap used in the experiments very well.

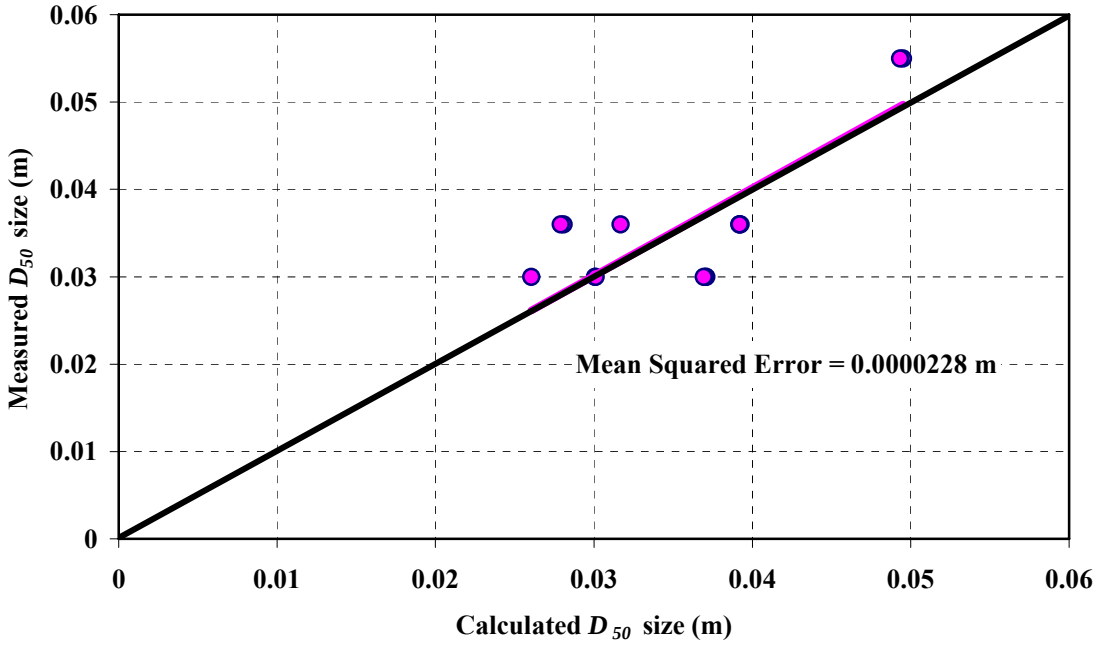

Figure 55. Graph. Validation of D_{50} for riprap sizing.

USE OF CROSS VANES FOR INLET SCOUR CONTROL

Rosgen-type cross vanes, used near the modeled culvert entrance in the approach flow, were tested as a countermeasure for mitigation of inlet culvert scour and channel instability. The original intent of this set of experiments was to optimize cross vane geometry and location to minimize the amount of inlet scour. After determining that the cross vanes promoted more scour, the listed cross vane experiments were replaced with experiments using streamlined wingwalls at the exit. Figures 56 and 57 show the configuration and dimensions of the cross vanes, and figure 58 shows the fabrication of the cross vane. Figure 59 shows a photo of the culvert and cross vane before the experiment was run.

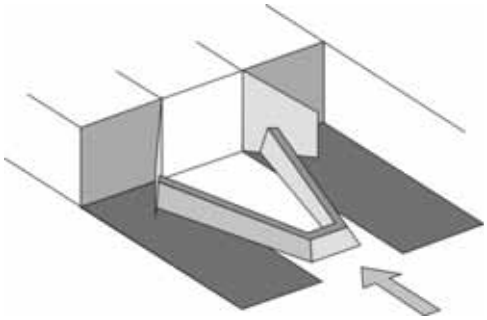

Figure 56. Diagram. Culvert with a cross vane.

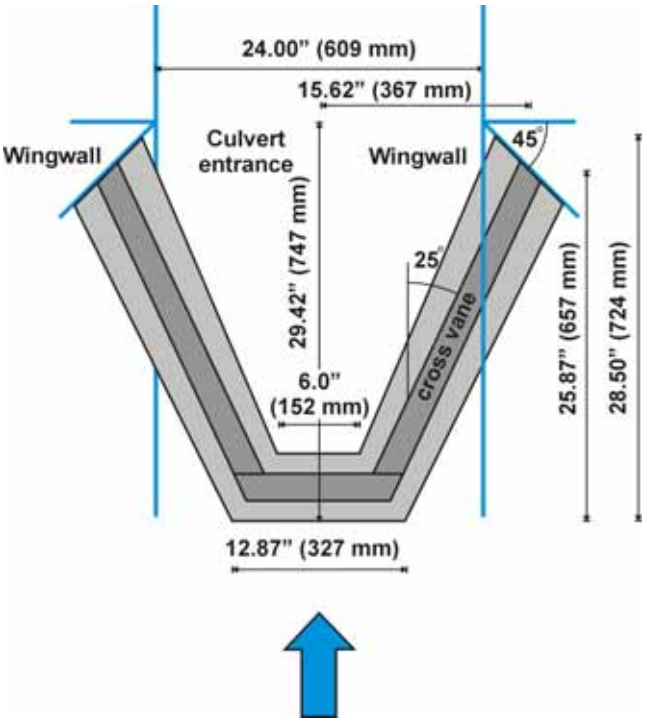

Figure 57. Diagram. Experimental arrangement of culvert with a cross vane.

Figure 58. Photo. Fabrication of the cross vane.

Figure 59. Photo. Cross vane installed at inlet of experimental culvert.

The cross vane contributed to, rather than diminished, the effect of scour at the inlet. The cross vane creates a spiral current on each side of the cross vane and excavates the corners, the opposite of its desired intent. The flow field was measured at the entrance with PIV and the results show the spiral current effect (figure 60). Figure 61 shows that scour is increased when the cross vane is added.

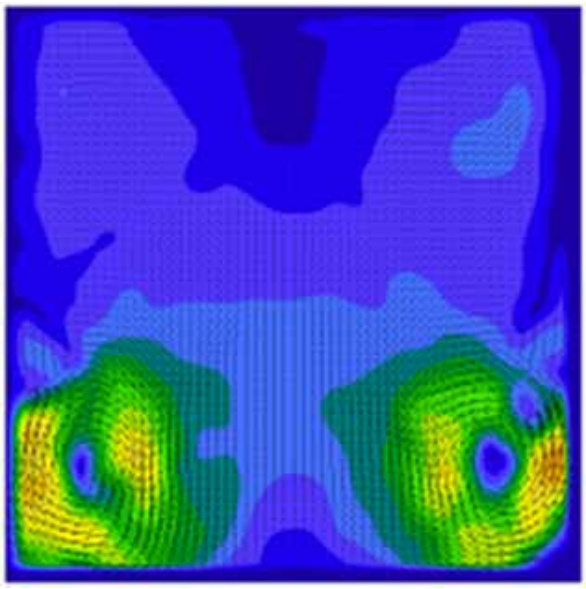

Figure 60. Image. PIV image of flow field at culvert entrance showing spiral current in corners.

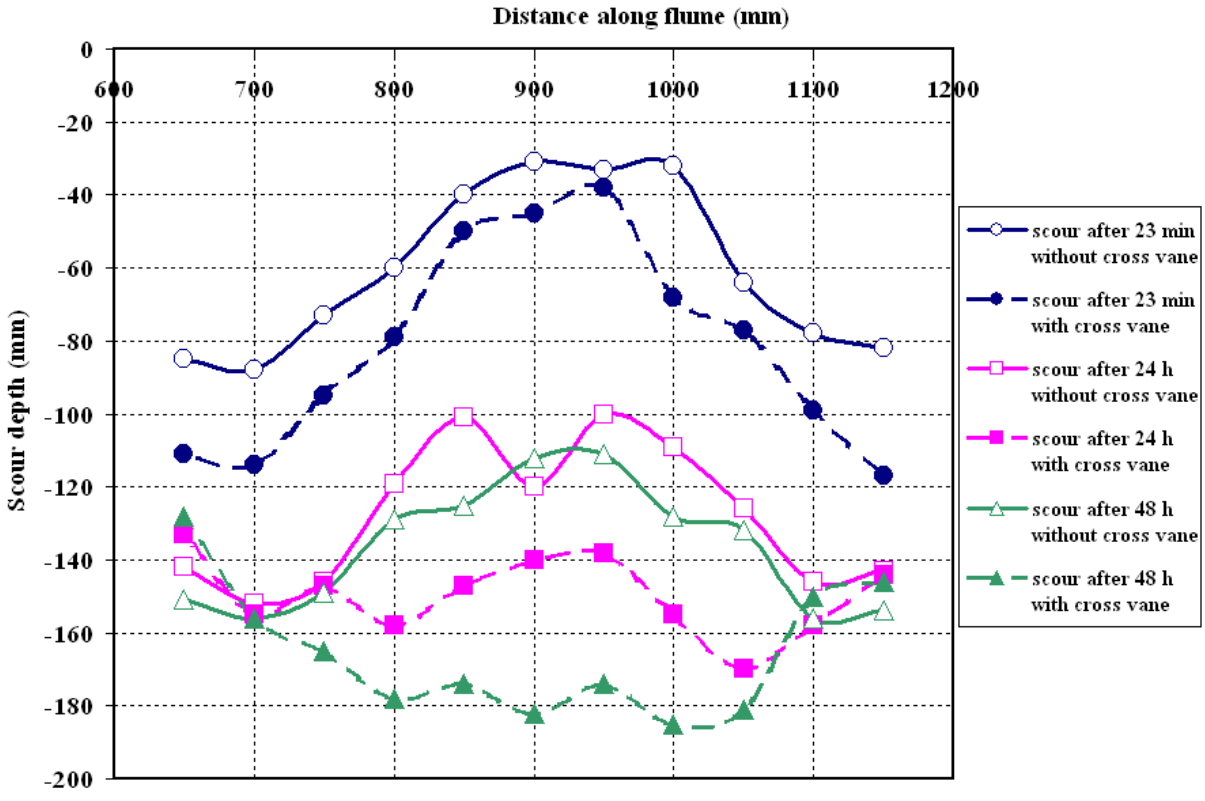

Figure 61. Graph. Cross vane results.

5. CONCLUSIONS

Phase II improved on the Phase I study results by providing additional research data, including the following.

- Additional riprap tests improved the riprap analysis. More data were developed, including data from experiments with wingwalls and under submerged conditions.

- Fixed-bed experiments accurately measured initial flow distributions and flow redistribution in the culvert. One of the problems encountered with the movable-bed experiments was that conditions change as soon as the experiments begin. The information from the fixed-bed experiments was used to validate three approximations of the representative velocity.

- Different outlet wingwall shapes were used to analyze outlet scour. Results from the observed outlet scour experiments are presented in spatial maps in appendix A.

- Many different theoretical approaches were used to help the practitioner calculate the maximum scour under unsubmerged flow conditions. However, the results for submerged bottomless culverts are only preliminary.

Equations are presented to estimate the maximum expected scour depths at the upstream corners of bottomless culverts under clear-water conditions. New equations are also presented to estimate the riprap sizes needed to protect bottomless culvert footings from scour.

All experiments outlined in the test matrix in table 1 were completed in Phase II, but there were some limitations in the experimental setup. The experimental results were based on laboratory flume experiments with a flat approach cross section with uniform flow conveyance, which is not typical of field conditions. The experiments were also conducted under clear-water approach flow conditions with no sediment being transported into the culvert. The authors attempted to present the results in terms of overbank flow rather than geometric variables; presenting the results is this fashion allows accounting for the reduced conveyance that is typical of overbank flow for natural streams. These results have not been tested for field conditions; however, they are offered as initial guidance for field applications. An anticipated next step is that MDSHA will adopt the results as preliminary design guidelines and test them for field sites using engineering judgment to decide if the applications are reasonable.

The abutment scour concept of using the flow distribution at the culvert entrance to compute the primary scour depth component and adjusting that with an empirical factor based on laboratory data appears to be valid for bottomless culverts. Three different equations for the initial representative velocity and two different equations for the critical incipient motion velocity were tested to compute the flow distribution scour. The Froude numbers in the experiments did not cover the full range that is expected in the field, and the negative slopes presented in table 2 are probably not realistic. In fact, other

experiments performed by GKY and Associates, Inc., show that the correlation of k_S with the Froude number is positive.[3] For this reason, we recommend changing the Froude number multiplier to zero for equations in table 2 with negative slopes. This change is equivalent to changing the k_s equations with a Froude number in them so that k_s equals only the intercept. Nevertheless, the laboratory data suggest that calculations of k_s as a function of either V_{RA}, V_{CL}, and F_1 or V_{RM}, V_{CN}, and $Q_{blocked}$ are the two best functions for calculating scour in an unsubmerged bottomless culvert. The k_p results, however, are still too preliminary to suggest the best predictors of scour in submerged bottomless culverts.

The culvert entrance flow conditions were a significant influence on the scour. The flow through various inlet and outlet configurations was investigated as both submerged (pressure flow) and unsubmerged to determine the overall effects of the flow conditions on scour hole formation. The results show that submerged flow conditions induce greater inlet scour depths, while unsubmerged flow conditions induce greater outlet scour depths. The results also show that 45-degree inlet wingwalls are effective at reducing inlet scour, whereas 8-degree inlet wingwalls are not effective.

The outlet scour experimental results showed the effects of using different wingwall configurations at the outlet. Changing the angle of the wingwalls reduces the turbulent shear stress, and thus reduces the scour depth created. The outlet experiments clearly demonstrate that outlet scour can be substantially reduced by using outlet wingwalls with a streamlined shape. The elongated streamlined bevel wingwall was best at reducing scour. Experimental results indicate that turbulence is reduced and "vortex shedding" caused by abrupt changes in pressure is almost eliminated by using this shape. In other words, the streamlined wall eliminates flow separation and decreases turbulence.[10] Hence, with the streamlined bevel, vortices do not propagate downstream and the resulting turbulence is more evenly distributed—not concentrated in a single location. Conversely, the abrupt change in pressure that results from a square exit shape (as found in culverts without wingwalls at the outlet) induces vortex shedding and increased scour depths.

Eight-degree outlet wingwalls were also tested because streamlined wingwalls may not be practical in the field. These results revealed reduced turbulence and scour depth at the outlet. This is an encouraging finding because wingwalls with an 8-degree flare are easy to construct or can be ordered prefabricated, which may make this design more cost-effective than the streamlined design.

Equation 27 is useful for sizing riprap to reduce scour. Chang's pile dissipators dissipated some of the energy at the outlet and thus reduced the scour depth. The MDSHA Standard Plan for countermeasures did not significantly reduce the scour depth, but it is considered a good practice because the riprap that was employed in this plan moved and fell into the scour holes, after which the riprap stabilized. However, since these results are still preliminary, this report does not make any recommendations about sizing or placing riprap for this design. Cross vanes are not recommended at the inlet because the results show that they contribute to rather than hinder scour due to a spiral current effect.

Additional research could extend and improve upon the Phase I and Phase II study results. This research could include:

- *Conceptual sediment balance relationships to extend the analysis to live-bed conditions.* The authors propose that Laursen's "sediment-in equals sediment-out" logic (that the amount of sediment entering a stream segment must equal the amount of sediment exiting) should apply with reasonable assumptions about flow distributions. An inherent assumption is that the empirical adjustment factors from the clear-water experiments can be applied to live-bed conditions. Live-bed flume experiments with sediment transport in the main channel and clear water (no sediment) in overbank flow are needed to test these assumptions.

- *Derivation of a safety factor to envelop the experimental riprap data.* Engineers often find that they use the same class of riprap for a wide range of requirements. A safety factor provides a level of confidence in applying engineering judgment in these situations.

6. SCOUR CALCULATION EXAMPLES

This section gives step-by-step instructions for calculating the maximum scour depth for unsubmerged bottomless culverts. Two different scenarios from the results section will be shown.

USING k_S AS A FUNCTION OF V_{RA}, V_{CL}, AND F_1

The first example is based on using V_{RA}, V_{CL}, and F_1. The procedure is as follows:

Step 1: Compute the representative velocity of the flow using the average velocity in the approach section (equation 2) as follows.

$$V_{RA} = \frac{Q}{A_{CULV}} = \frac{Q}{y_0 \, w_{CULV}} \tag{28}$$

where:

Q is volumetric flow through the culvert (m^3/s).
y_0 is depth of flow in the approach to the culvert before scour (m).
w_{CULV} is width of the culvert inlet (m).

Step 2: Express the critical velocity computed by Laursen's method (equation 5) in terms of y_2 as follows.

$$V_{CL} = 6.19 \, y_2^{1/6} \, D_{50}^{1/3} \tag{29}$$

where:

y_2 is equilibrium flow depth (m).
D_{50} is sediment size (m).

Step 3: Everything in the previous two equations should be known except for y_2. Now we can substitute the previous two equations into equation 1 as follows.

$$y_2 = \frac{V_{RA} \, y_0}{V_{CL}} = \frac{Q \, y_0}{y_0 \, w_{CULV} \, (6.19 \, y_2^{1/6} \, D_{50}^{1/3})} \tag{30}$$

This expression can now be rearranged to calculate y_2 as follows.

$$y_2 = \left(\frac{Q \, y_0}{6.19 \, y_0 \, w_{CULV} \, D_{50}^{1/3}} \right)^{6/7} \tag{31}$$

Step 4: Now use the scour equations from the first entry (k_S) in table 2 to calculate the maximum scour, recalling that only the intercept of these equations should be used.

Without wingwalls, the maximum scour is computed with the following equation.

$$y_{max} = 2.2658\, y_2 = 2.2658\left(\frac{Q\, y_0}{6.19\, y_0\, w_{CULV}\, D_{50}^{1/3}}\right)^{6/7} \tag{32}$$

Alternatively, the equation for the maximum scour with wingwalls is as follows.

$$y_{max} = 1.7613\, y_2 = 1.7613\left(\frac{Q\, y_0}{6.19\, y_0\, w_{CULV}\, D_{50}^{1/3}}\right)^{6/7} \tag{33}$$

USING k_S AS A FUNCTION OF V_{RM}, V_{CN}, AND $Q_{blocked}$

The second example is based on using V_{RM}, V_{CN}, and $Q_{blocked}$. The procedure is as follows:

Step 1: Compute representative velocity of the flow using the calibrated velocity in the culvert inlet (equation 22) as follows.

$$V_{RM} = \left[1.024\left(\frac{q_1}{q_2}\right)^{1.5} + 1.28\right]\left[\frac{Q}{y_0 w_{CULV}}\right] \tag{34}$$

where:

Q	is volumetric flow through the culvert (ft^3/s or m^3/s).
y_0	is depth of flow in the approach to the culvert before scour (ft or m).
w_{CULV}	is width of the culvert inlet (ft or m).
q_1	is unit discharge in the approach section (ft^2/s or m^2/s).
q_2	is unit discharge in the contracted section (ft^2/s or m^2/s).

Note that the unit discharge ratio of q_1 divided by q_2 can be computed from a width ratio as follows.

$$\frac{q_1}{q_2} = \frac{w_{CULV}}{w_a} \tag{35}$$

where:

w_{CULV}	is width of the bottomless culvert inlet (m).
w_a	is width of the approach section to the culvert (m).

Step 2: Express the critical velocity computed by Neill's method (equations 6, 7, and 8, or 9) in terms of y_2. For example, for D_{50} sediment size greater than 0.0003 m (0.001 ft) but less than 0.03 m (0.1 ft), the equation for Neill's critical velocity is given as follows.

$$V_{CN} = K_{U1}\, 11.5\, y_2^{\,x}\, D_{50}^{\,0.35} \tag{36}$$

The exponent, x, is calculated using equation 37:

$$x = K_{U2}\frac{0.123}{D_{50}^{\,0.20}} \tag{37}$$

where:

y_2	is equilibrium flow depth, m or ft.
D_{50}	is sediment size, m or ft.
K_{U1}	is $0.3048^{(0.65-x)}$ for SI units, or 1.0 for U.S. customary units.
x	is the exponent from equation 8.
K_{U2}	is 0.788 for SI units, or 1.0 for U.S. customary units.

Step 3: Everything in the previous three equations should be known except for y_2. Now we can substitute the previous two equations into equation 1 as follows.

$$y_2 = \frac{V_{RM}\, y_0}{V_{CN}} = \frac{(1.024(q_1/q_2)^{1.5} + 1.28)\, Q\, y_0}{y_0\, w_{CULV}\, (11.5 K_{U1}\, y_2^{\,x}\, D_{50}^{\,0.35})} \tag{38}$$

This expression can now be rearranged to calculate y_2 as follows.

$$y_2 = \left[\frac{(1.024(q_1/q_2)^{1.5} + 1.28) Q}{11.5 K_{U1}\, w_{CULV}\, D_{50}^{\,0.35}}\right]^{\frac{1}{1+x}} \tag{39}$$

Step 4: Now use the scour equations from the first entry (k_S) in table 2 to calculate the maximum scour.

Without wingwalls, the maximum scour is computed with the following equation.

$$y_{max} = 1.5149\left(\frac{Q_{blocked}}{\sqrt{g}\, y_2^{\,5/2}}\right)^{0.0602}\left[\frac{(1.024(q_1/q_2)^{1.5} + 1.28)\, Q}{11.5 K_{U1}\, w_{CULV}\, D_{50}^{\,0.35}}\right]^{\frac{1}{1+x}} \tag{40}$$

Alternatively, the equation for the maximum scour with wingwalls is as follows.

$$y_{max} = 1.4456\left(\frac{Q_{blocked}}{\sqrt{g}\, y_2^{\,5/2}}\right)^{0.2332}\left[\frac{(1.024(q_1/q_2)^{1.5} + 1.28)\, Q}{11.5 K_{U1}\, w_{CULV}\, D_{50}^{\,0.35}}\right]^{\frac{1}{1+x}} \tag{41}$$

APPENDIX A. SCOUR MAPS

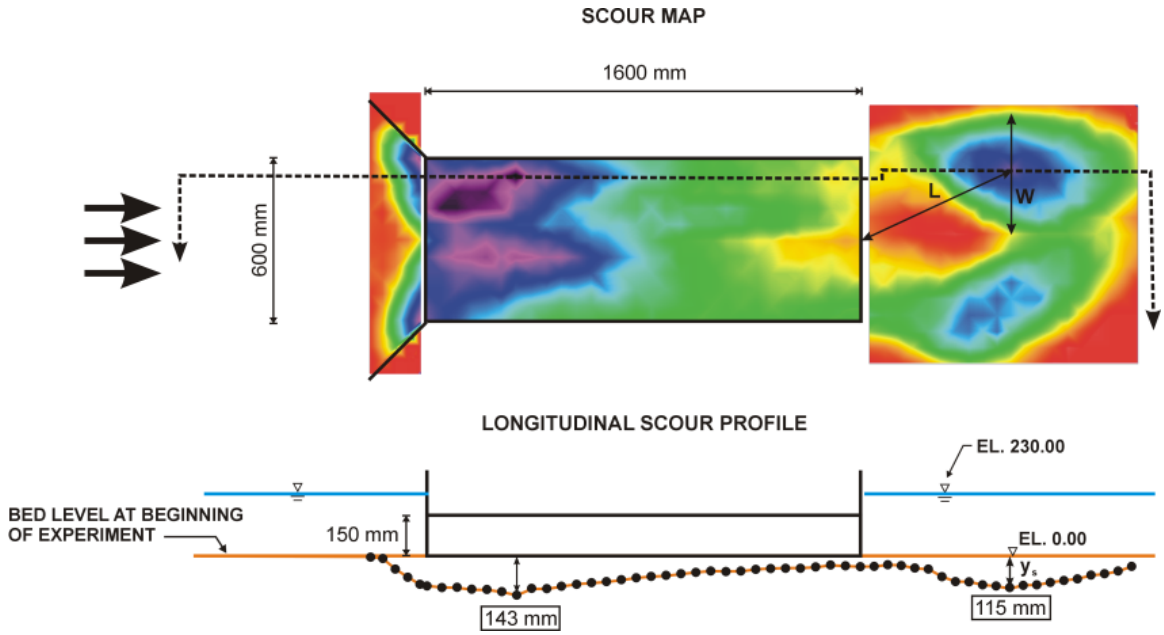

Note: D_{50} is 2 mm; the depth of the water, h, is 23 cm; the velocity, V, is 14 cm/s.

Figure 62. Diagram. Scour map (top) and profile (bottom), culvert submerged, February 11, 2003.

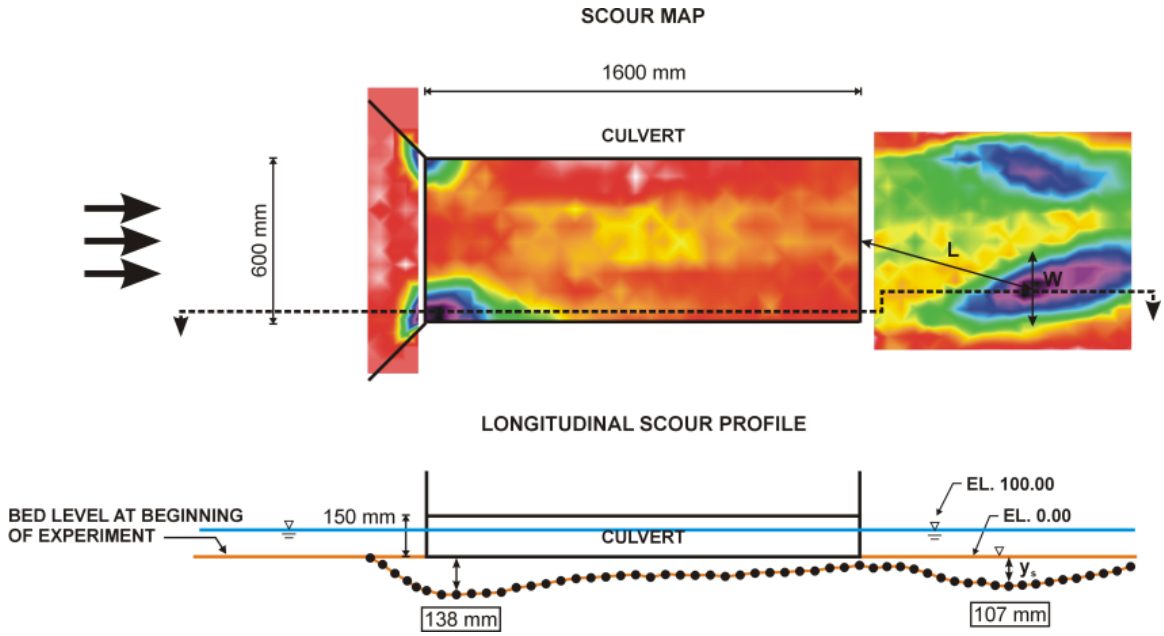

Note: D_{50} is 2 mm; the depth of the water, h, is 10 cm; the velocity, V, is 14 cm/s.

Figure 63. Diagram. Scour map (top) and profile (bottom), free surface, February 25, 2003.

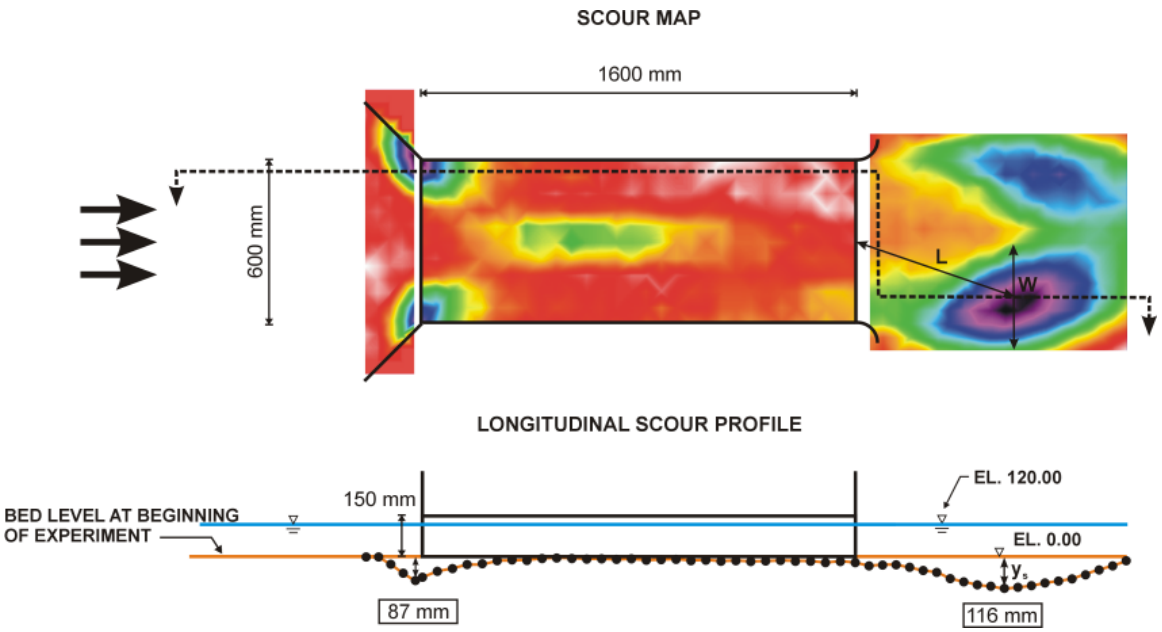

Note: D_{50} is 2 mm; the depth of the water, h, is 12 cm; the velocity, V, is 15 cm/s.

Figure 64. Diagram. Scour map (top) and profile (bottom), free surface with circular bevel at exit, March 25, 2003.

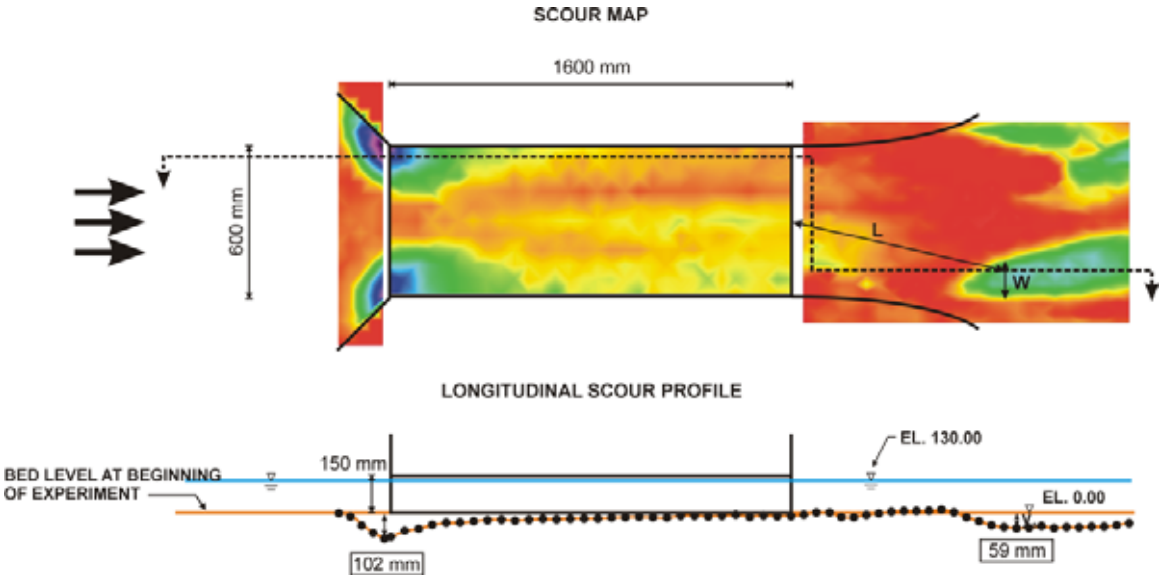

Note: D_{50} is 2 mm; the depth of the water, h, is 13 cm; the velocity, V, is 16 cm/s.

Figure 65. Diagram. Scour map (top) and profile (bottom), free surface with streamlined bevel at exit, April 7, 2003.

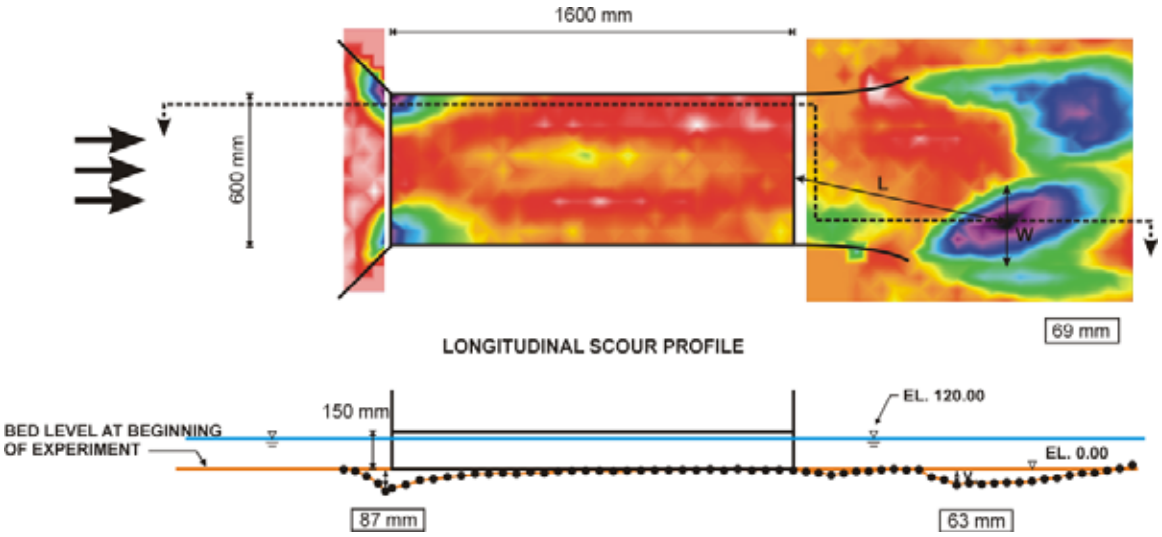

Note: D_{50} is 2 mm; the depth of the water, h, is 12 cm; the velocity, V, is 15 cm/s.

Figure 66. Diagram. Scour map (top) and profile (bottom), free surface with short streamlined bevel at exit, April 29, 2003.

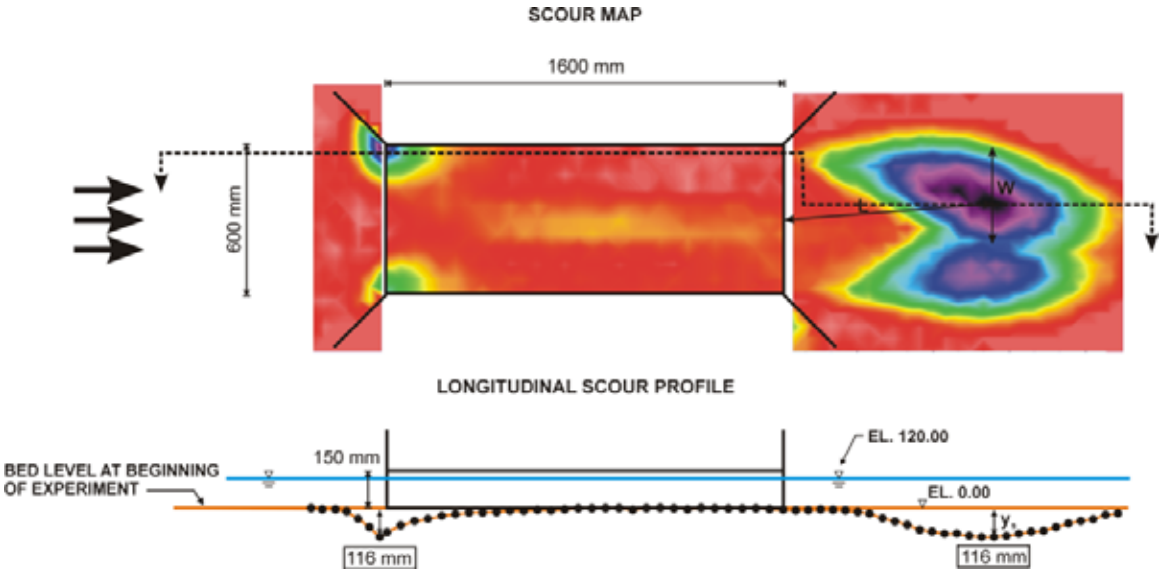

Note: D_{50} is 2 mm; the depth of the water, h, is 12 cm; the velocity, V, is 15 cm/s.

Figure 67. Diagram. Scour map (top) and profile (bottom), free surface with wingwalls at outlet, July 22, 2003.

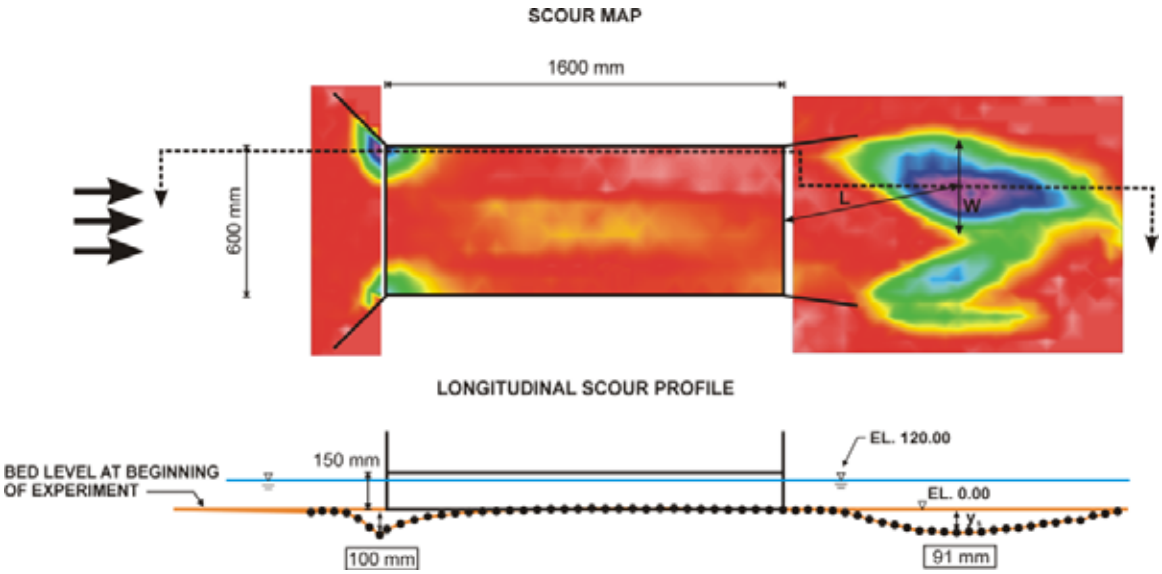

Note: D_{50} is 2 mm; the depth of the water, h, is 12 cm; the velocity, V, is 15 cm/s.

Figure 68. Diagram. Scour map (top) and profile (bottom), free surface with 8-degree wingwalls at outlet, August 6, 2003.

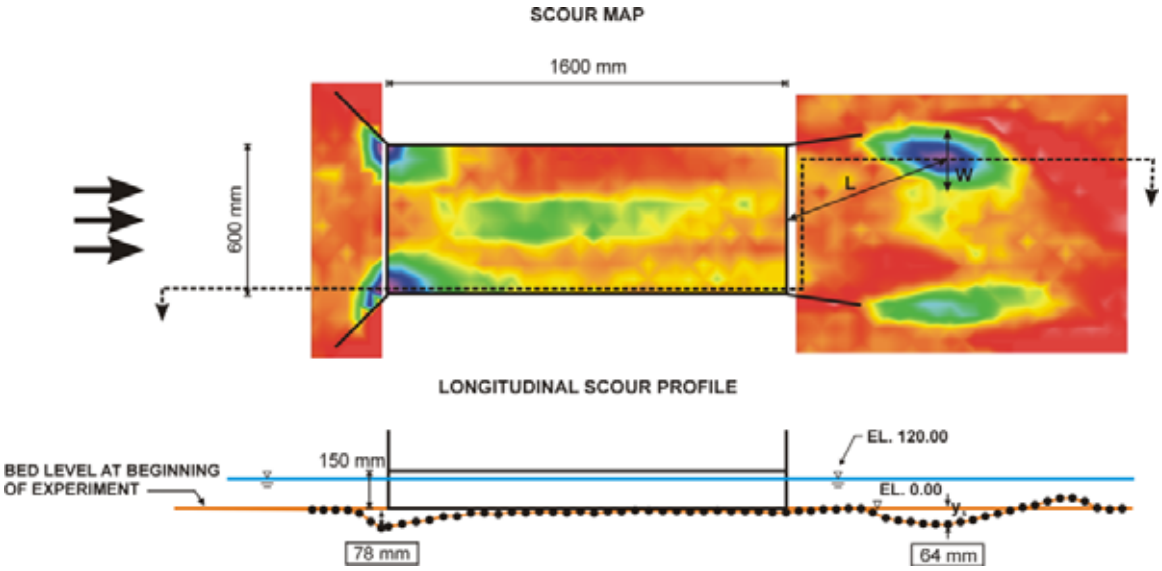

Note: D_{50} is 2 mm; the depth of the water, h, is 12 cm; the velocity, V, is 15 cm/s.

Figure 69. Diagram. Scour map (top) and profile (bottom), free surface with 8-degree wingwalls at outlet (smooth walls), October 7, 2003.

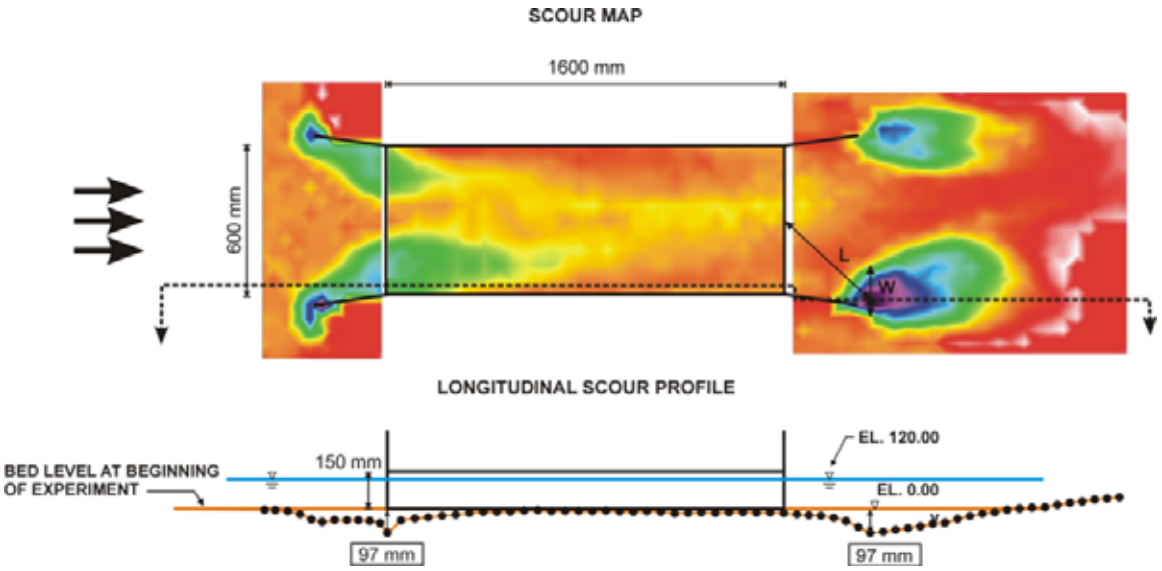

Note: D_{50} is 2 mm; the depth of the water, h, is 12 cm; the velocity, V, is 15 cm/s.

Figure 70. Diagram. Scour map (top) and profile (bottom), free surface with 8-degree wingwalls at outlet and inlet (smooth walls), December 9, 2003.

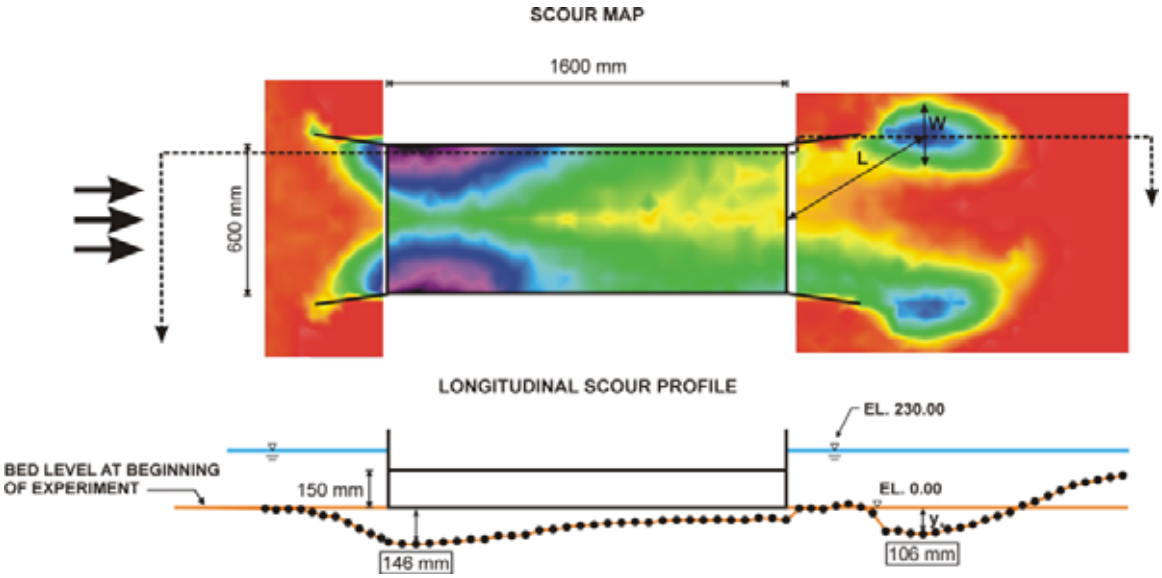

Note: D_{50} is 2 mm; the depth of the water, h, is 23 cm; the velocity, V, is 14 cm/s.

Figure 71. Diagram. Scour map (top) and profile (bottom), submerged with 8-degree wingwalls at outlet and inlet (smooth walls), December 16, 2003.

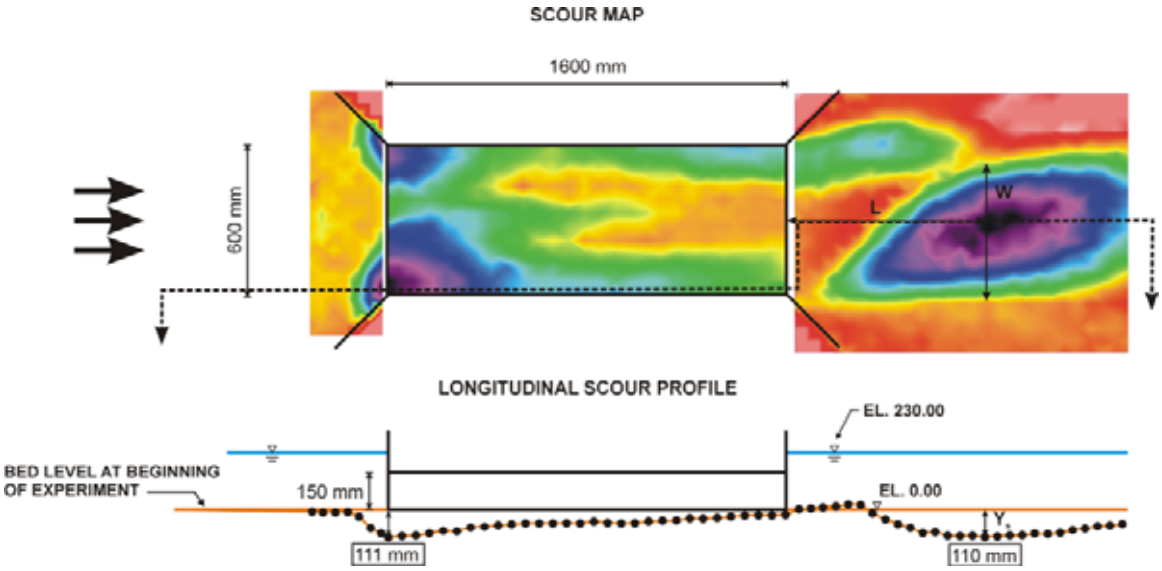

Note: D_{50} is 2 mm; the depth of the water, h, is 23 cm; the velocity, V, is 13 cm/s.

Figure 72. Diagram. Scour map (top) and profile (bottom), submerged with 45-degree wingwalls at outlet and inlet, October 27, 2004.

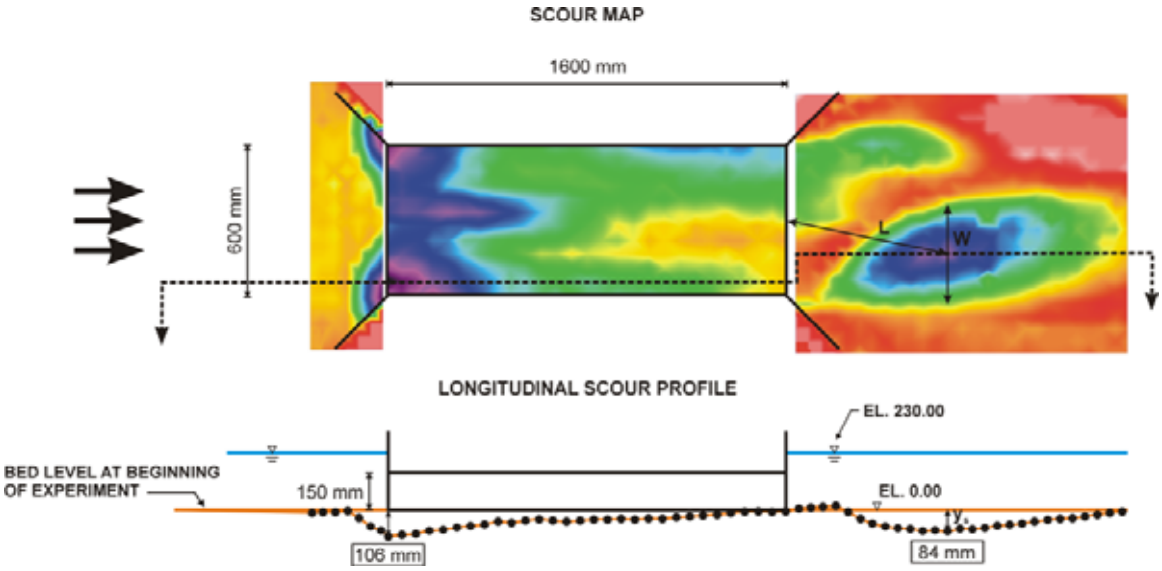

Note: D_{50} is 2 mm; the depth of the water, h, is 23 cm; the velocity, V, is 13 cm/s.

Figure 73. Diagram. Scour map (top) and profile (bottom), submerged with 45-degree wingwalls at outlet and inlet and Chang's pile dissipater at outlet, November 10, 2004.

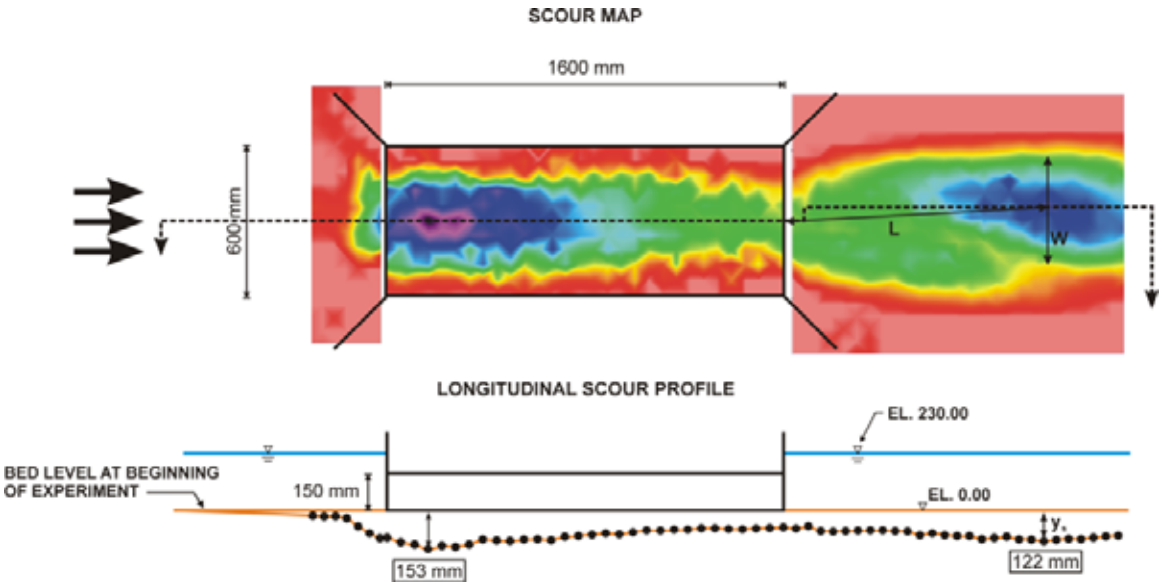

Note: D_{50} is 2 mm; the depth of the water, *h*, is 23 cm; the velocity, *V*, is 13 cm/s; the discharge is 0.054 m^3/s; the riprap is 25.4 mm.

Figure 74. Diagram. Scour map (top) and profile (bottom), MDSHA Standard Plan, submerged with 45-degree wingwalls at outlet and inlet, March 19, 2004.

APPENDIX B. OUTLET SCOUR RESULTS

Table 8. Outlet scour results summary.

Date	Figure	Flow Depth [cm]	Velocity [cm/s]	Sub-merged	Inlet Wingwall	Outlet Wingwall	Note	Width of Scour Hole (*W*) [mm]	Depth of Scour Hole (*ys*) [mm]	Distance to Scour Hole (*L*) [mm]
2/11/2003	62	23	14	Yes	45 degree	None	Bottomless culvert study	446	115	615
2/25/2003	63	10	14	No	45 degree	None	Bottomless culvert study	278	107	659
3/25/2003	64	12	15	No	45 degree	Circular bevel	Bottomless culvert study	388	116	618
4/7/2003	65	13	16	No	45 degree	Elongated, streamlined bevel	Bottomless culvert study	157	59	875
4/29/2003	66	12	15	No	45 degree	Short streamlined bevel	Bottomless culvert study	330	63	874
7/22/2003	67	12	15	No	45 degree	45 degree	Bottomless culvert study	393	116	846
8/6/2003	68	12	15	No	45 degree	8 degree (rough)	Bottomless culvert study	323	91	516
10/7/2003	69	12	15	No	45 degree	8 degree (smooth)	Bottomless culvert study	249	64	676
12/9/2003	70	12	15	No	8 degree (smooth)	8 degree (smooth)	Bottomless culvert study	212	97	470
12/16/2003	71	23	14	Yes	8 degree (smooth)	8 degree (smooth)	Bottomless culvert study,	258	106	648
10/27/2004	72	23	13	Yes	45 degree	45 degree	HGL (hydraulic grade line) for bottomless culverts	556	110	803
11/10/2004	73	23	13	Yes	45 degree	45 degree	HGL for bottomless culverts, Chang's pile dissipator at outlet	403	84	663
3/19/2004	74	23	13	Yes	45 degree	45 degree	MDSHA Standard Plan, Riprap = 1"	441	122	1,070

REFERENCES

1. Kerenyi, K., Jones, J. S., and Stein, S., *Bottomless Culvert Scour Study: Phase I Laboratory Report*, Federal Highway Administration, Report Number FHWA-RD-02-078, McLean, VA, November 2003.

2. Chang, F., and Davis, S., "Maryland Procedure for Estimating Scour at Bridge Abutments, Part 2—Clear Water Scour," *Proceedings of the International Water Resources Engineering Conference*, ASCE, Memphis, TN, Vol. 1, pp. 169–173, 1998.

3. Young, G. K., Dou, X., Saffarina, K., and Jones, J. S., (GKY and Associates. Inc.), "Testing Abutment Scour Model," *Proceedings of the International Water Resources Engineering Conference*, ASCE, Memphis, TN, Vol. 1, pp. 180–185, 1998.

4. Sturm, T. W., and Chrisochoides, A., "Abutment Scour in Compound Channels for Variable Setbacks," *Proceedings of the International Water Resources Engineering Conference*, ASCE, Memphis, TN, Vol. 1, pp. 174–179, 1998.

5. Maryland State Highway Administration, Office of Bridge Development, *ABSCOUR Users Manual*, version 7, build 1.0, August 1, 2005.

6. Federal Highway Administration, *Evaluating Scour at Bridges*, Hydraulic Engineering Circular No. 18, 4th ed., Washington, DC, 2001.

7. Neill, C. R., *Guide to Bridge Hydraulics*, University of Toronto Press, Toronto, Canada, 1973.

8. Mahmood, K., and Shen, H. W., "Regime Concept of Sediment-Transporting Canals and Rivers," *River Mechanics*, H. S. Shen, ed., Vol. II, H. W. Shen, Fort Collins, CO, pp. 30–1 to 30–39, 1971.

9. Ishbash, S. V., *Construction of Dams by Depositing Rock in Running Water*, Second Congress on Large Dams, Communication No. 3, Washington, DC, 1936.

10. Rouse, H. (ed.), *Engineering Hydraulics: Proceedings of the Fourth Hydraulics Conference, Iowa Institute of Hydraulics Research, June 12–15, 1949*, John Wiley & Sons, Inc., New York, NY, 1950.

HRDI-07/2-07(WEB)E